Environmental Systems Research

RESEARCH

Open Access

Integrated use of the CA–Markov model and the Trends.Earth module to enhance the assessment of land cover degradation

Henry M. Zimba[1,2*], Kawawa E. Banda[2], Stephen Mbewe[2] and Imasiku A. Nyambe[2]

Abstract

This study aims to demonstrate the potential of assessing future land cover degradation status by combining the forecasting capabilities of the Cellular-Automata and Markov chain (CA-Markov) models in Idris Selva with the land cover degradation (LCD) model in the Trends.Earth module. The study focuses on the upper Zambezi Basin (UZB) in southern Africa, which is one of the regions with high rates of land degradation globally. Landsat satellite imagery is utilised to generate historical (1993–2023) land cover and land use (LCLU) maps for the UZB, while the global European Space Agency Climate Change Initiative (ESA CCI) LCLU maps are obtained from the Trends.Earth module. The CA-Markov chain model is employed to predict future LCLU changes between 2023 and 2043. The LCD model in the Trends.Earth module in QGIS 3.32.3 is then used to assess the historical and forecasted land cover degradation status. The findings reveal that land cover degradation maps produced from local LCLU classifications provide more detailed information compared to those produced from the global ESA CCI LCLU product. Between 2023 and 2043, the UZB is predicted to experience a net reduction of approximately 3.2 million hectares of forest cover, with an average annual reduction rate of – 0.13%. In terms of land cover degradation, the UZB is forecasted to remain generally stable, with 87% and 96% of the total land cover area expected to be stable during the periods 2023–2033 and 2033–2043, respectively, relative to the base years 2023 and 2033. Reduction in forest cover due to the expansion of grassland, human settlements, and cropland is projected to drive land cover degradation, while improvements in forest cover are anticipated through the conversion of grassland and cropland into forested areas. It appears that using locally produced LCLU with high-resolution images provides better assessments of land degradation in the Trends.Earth module than using global LCLU products. By leveraging the opportunities offered by models with capacity to predict LCLU such as the CA–Markov model and the capabilities of the LCD model, as evidenced in this study, valuable forecasted information can be effectively obtained for monitoring land cover degradation. This information can then be used to implement targeted interventions that align with the objective of realising the United Nations' land degradation neutral world target by 2030.

Keywords CA–Markov model, Land cover and land use, Land cover degradation, Land cover degradation model, Trends.Earth module, Upper Zambezi Basin

*Correspondence:
Henry M. Zimba
henryzimba@yahoo.co.uk
[1] Department of Agriculture, Ministry of Agriculture, Mulungushi House, Independence Avenue, P.O. Box 50595, Lusaka, Zambia
[2] Integrated Water Resources Management Centre, Department of Geology, School of Mines, University of Zambia, Great East Road Campus, Lusaka, Zambia

Introduction

Globally, land degradation is on the rise, primarily as a result of changes in land cover and land use (LCLU). These changes are especially evident in the conversion of forests into cropland and settlements (Potapov et al. 2022; Hu et al. 2021; Winkler et al. 2021; Bär et al. 2023). Surprisingly, it has been discovered that global land cover

and land use changes are actually four times greater than previously estimated, largely due to uncertainties in the methods and data sets used (Winkler et al. 2021). The region's most severely affected by land degradation include Africa south of the equator, which accounts for 13% of the global degrading area and 18% of net primary productivity (Lewandowski et al. 2013). Biophysical and socioeconomic interactions in semi-arid regions are complex, resulting in effects such as altered land cover, land use, and degraded landscape structures (Chundu et al. 2024; Phiri et al. 2019; Gebresamuel et al. 2010). Therefore, the detection of LCLU changes has become a matter of concern for environmentalists, conservationists, and land use planners, given its significant impact on natural ecosystems (Chundu et al. 2024; Arfasa et al. 2023; Lukas et al. 2023). The efficacy of remedial interventions may be compromised depending on the extent of these interactions. Most interventions rely on historical detection of changes in LCLU, which can hinder effective remedial outcomes due to potential differences in future changes to the landscape structure (Kgaphola et al. 2023; Ukhurebor et al. 2022; Bajocco et al. 2012). The United Nations (UN) seeks to achieve a "land degradation neutral (LDN) world" by 2030 as part of Sustainable Development Goal (SDG) 15. The UN defines land degradation neutrality (LDN) as "a state whereby the amount and quality of land resources necessary to support ecosystem functions and services and enhance food security remain stable or increase within specified temporal and spatial scales and ecosystems" (Orr et al. 2017) The Sustainable development goal (SDG) 15 adopted the LDN as one of the targets to guide the framing of the United Nations Convention to Combat Desertification (UNCCD) (Cowie et al. 2018). The Trends.Earth module (Trends.Earth 2022) to support reporting to the Global Environment Facility (GEF) and UNCCD is a free and open-source tool designed to facilitate the comprehensive understanding of land change, including land cover degradation. It provides users with the ability to access and integrate the most reliable and diverse data sources, ranging from globally available datasets to tailored local maps. By harnessing this wealth of information, Trends.Earth module enables users to delve into the intricacies of land change, unravelling the factors and motivations driving alterations on the ground. However, a limitation of the Trends.Earth module is that it currently only offers historical global land cover products up to the year 2020. This presents a challenge since the GEF and UNCCD monitoring framework intends to cover data up to the year 2030. Moreover, the scientific conceptual framework for LDN is "designed based on the counterbalancing mechanism to attain neutrality, which envisions and aspires to balance projected positive and negative changes" (Cowie et al. 2018). Furthermore, it is hypothesised that the utilisation of locally produced LCLU products for the evaluation of land degradation could result in higher precision compared to the application of global products (Tulbure et al. 2022; Wang et al. 2019) within the Trends.Earth module. Therefore, predictions of LCLU at a local or regional level offer a broader perspective for comprehensively understanding both past and potential future changes in LCD. This enables the formulation of more precise interventions and strategies to address these changes (Lukas et al. 2023; Tulbure et al. 2022; Wang et al. 2021; Cowie et al. 2018; Halmy et al. 2015; Roy et al. 2015).

Several approaches for detecting and predicting land cover and land use (LCLU) changes exist, among which the artificial neural network (ANN), cellular automata (CA), and Markov chain (MC) models appear to be the most commonly utilised (Lukas et al. 2023; Akdeniz and Sag 2022; Wang et al. 2021; Näschen et al. 2019; Mondal et al. 2019; Hamad et al. 2018; Halmy et al. 2015; Singh et al. 2015; Corner et al. 2014; Memarian et al. 2012). Some studies have used a combination of the CA-Markov models and the ANN to better prediction outcomes for particular landscapes (Lukas et al. 2023; Gharaibeh et al. 2020). However, in this study, we utilise only a combination of the CA and Markov chain models, known as CA-Markov, as described in Singh et al. 2015 and Memarian et al. 2012. We employ these models to predict LCLU changes using satellite images due to their immense flexibility and capabilities. Therefore, this study demonstrates the potential use of CA–Markov model LCLU outputs for predicting LCD at a local level, thus addressing the limitation of the Trends.Earth module in making forecasts. The forecasts at the local level are valuable not only for monitoring purposes, but also for informing targeted interventions aimed at mitigating LCD. The Upper Zambezi Basin (UZB) in Angola and Zambia encompasses the upstream region of the Zambezi River (Beilfuss 2012). The UZB is susceptible to climatic hazards such as droughts and floods, and has witnessed a rise in mining activities, population, and human settlements (Hughes and Farinosi 2020; Beilfuss 2012). Studies conducted in the Upper Zambezi Basin have primarily focused on the hydrology and ecology of the basin, particularly with regard to the associated climate implications (Chomba et al. 2022; Makungu and Hughes 2021; Zimba et al. 2018; Timberlake 2000). Some studies have also examined changes in Land Cover and Land Use (LCLU) within the Upper Zambezi Basin, both at a broader level and in specific areas of Angola (Kissanga et al. 2024) and Zambia (Banda et al. 2023; Tiamgne et al. 2021; Phiri et al. 2019; Shakachite et al. 2016). However, there has been a lack of research investigating the specific

LCLU changes occurring in the UZB catchment, as well as assessments of the historical and projected long-term degradation of land cover. These changes in LCLU within the UZB have significant implications for the sustainability of the ecohydrological functions of the Zambezi River Basin. It is essential to determine these changes in order to implement appropriate remedial measures. This study aimed to assess the utility of the forecasting capabilities of the CA–Markov model(s) and the LCD model in the Trends.Earth module to enhance our understanding of land cover degradation at a local level. The study assessed the historical and projected LCD in the UZB from 1993 to 2043, surpassing the target year of 2030 for reporting to the Global Environment Facility (GEF) and the United Nations Convention to Combat Desertification (UNCCD). The period from 1993 to 2023 has been well-documented as a time when land cover-altering activities, such as agriculture and mining, increased in both Angola and Zambia (Kissanga et al. 2024; World Bank 2010). This period also saw a significant rise in the human population in the region, which is a major driver of changes in land cover. The increase in population leads to higher agricultural production to meet food demands and the expansion of settlements (Phiri et al. 2019). Therefore, this period is particularly suitable for effectively detecting changes in land cover. Additionally, the period from 2023 to 2043 includes the timeframe for achieving Land Degradation Neutrality (LDN) as outlined in the sustainable development goals. These goals are expected to be achieved by the year 2030. The 13-year extension beyond 2030 serves as a projection to plan the management of the upper Zambezi Basin.

Data and methods

Study area

The UZB is the north western part of the Zambezi River Basin encompassing areas in north east of Angola and north west of Zambia. It stretches between longitude 18° E and 27° E and latitudes 10° S and 17° S in southern Africa (Fig. 1). The upper course of the Zambezi River is situated on an elevated plateau, which leads to relatively mild temperatures ranging between 18 and 30 °C due to the influence of altitude. In the winter months (May to July), the weather is cool and dry, with an average temperature of 20 °C. From August to October, there is a noticeable increase in average temperatures, just before

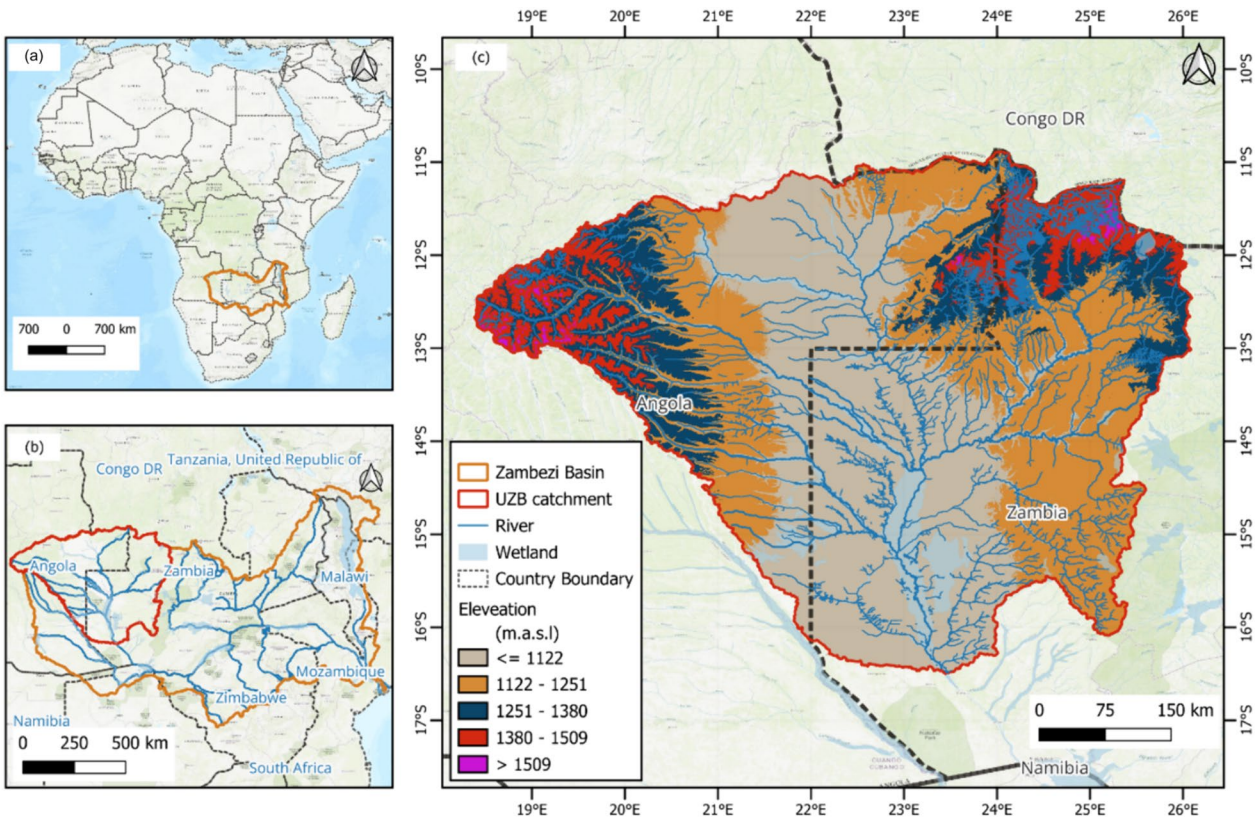

Fig. 1 Location of the study area in **a** Africa, **b** in Angola and Zambia in southern Africa, and **c** the spatial distribution of elevation using the ASTER digital elevation model, rivers and wetlands in the Upper Zambezi Basin catchment

the rainy season begins in October. During this period, temperatures can become excessively hot, often reaching 40 °C. The rainy season lasts from November to April and is characterised by short, intense thundershowers. Sometimes, the rate of rainfall can reach 150 mm per hour, followed by clear skies in between showers. It is during these months that the upper Zambezi receives the majority of its rainfall, resulting in significant variations in the river's flow throughout the year (Beilfuss 2012; Timberlake 2000). Some of the major rivers that drain the UZB include the Zambezi, Kabompo, Luanginga, Lungwebungu (Beilfuss 2012). The headwaters of the Zambezi, located in north eastern Angola and north western Zambia, are associated with the Congolian biome, which exhibits a more humid and warmer climate in comparison to the remaining parts of the Zambezi Basin (Fanshawe et al. 2010; Timberlake 2000). The flora and fauna in the UZB comprise a blend of species found in the forested Congo Basin and those inhabiting the less tropical, more wooded areas of the Zambezi Basin (Timberlake 2000). The Zambezian biome spans the remainder of the UZB and consists of woodland, grassland, swamp, and lakes. It experiences a strongly seasonal climate, characterized by a distinct dry season. The Zambezian biome can be further classified into wetter regions featuring miombo broad-leaved woodland, and drier regions with mopane or Acacia woodland (Fanshawe et al. 2010; Timberlake 2000). The UZB is also home to important wetlands such as the Barotse that support ecohydrological functions and various livelihoods (Makungu and Hughes 2021; Zimba et al. 2018; Fanshawe et al. 2010; Timberlake 2000). Over the years there has been increase in human settlements and mining activities in the UZB (Tiamgne et al. 2021; Kissanga et al. 2024; Mendelsohn 2019). These aspects have potential to degrade the landscape of the UZB. Land cover degradation in the landscape of the UZB has ability to negatively affect ecosystem services including tourism, food, hydro-power generation from reduced river flows as a result of changes in climate (Barati et al. 2023).

Data

The data, methods/processes, and outputs of this study are depicted in Fig. 2. Both satellite and field-based data were utilized in the study.

Satellite imagery

The Landsat satellite data was selected due to the presence of an extensive and reliable archive of high-quality historical data, dating back to 1984 in the specific case of the data utilised in this study. This data offers a relatively high spatial resolution of 30 m. The spectral characteristics of the Landsat data used in the study can be found in the following documentation (Lulla et al. 2021; Roy et al. 2014; Chander and Markham 2003).

Satellite data pre-processing and quality control

To reduce errors, this study utilized pre-processed Landsat 5 Thematic Mapper (TM), Landsat 8 Operational Land Imager and Thermal Infrared Sensor (OLI-TIRS), and Landsat 9 OLI-TIRS top of atmosphere (TOA) reflectance products obtained from the United States Geological Survey (USGS) through the Climate Engine (https://app.climateengine.org/; last accessed 25/07/2023). Additionally, all Landsat data were projected in the same manner. The average TOA reflectance for the months of June to August during the dry season was used.

This period was selected because it is easier to separate the grass component from the forest (tree) when the grass dries out and trees have not completely shed their leaves, especially in the areas covered by miombo woodland. The study followed recommended practices, including image mosaicking and compositing. The software platforms used in the study were ArcGIS 10.7, IDRIS Selva 17, and QGIS 3.32.3.

LCLU classification scheme

The LCLU classification scheme utilised in this study was developed by merging the classification schemes of the Food and Agriculture Organisation (FAO) (Latham et al. 2002) and the Forestry Department of Zambia (Vesa et al. 2013). The scheme was established after conducting an initial assessment of the predominant LCLU types and evaluating the distinguishability of the spectral signatures for the various LCLU types in the study area. Initially, eight LCLU classes were chosen, which were subsequently reduced to five using the reclassification tool in Idris Selva. This reduction aimed to enhance both the accuracy and change assessment. The resulting five classes were: forest, grassland, cropland, built-up/bareland, and water body.

Selection of LCLU classification model

The study used the maximum likelihood approach (Ahmad and Quegan 2012; Perumal and Bhaskaran 2010) to create the LCLU (Land Cover and Land Use) maps. This approach was selected because it is widely used in LCLU classification and has consistently proven to produce accurate results in various studies worldwide (Norovsuren et al. 2019; Shivakumar and Rajashekararadhya 2018; Karan and Samadder 2018; Lam et al. 2008).

Acquisition of training data and band selection

The LCLU classification was based on regions of interest (ROIs), also known as training areas, for each class. ROIs were selected based on their uniformity and

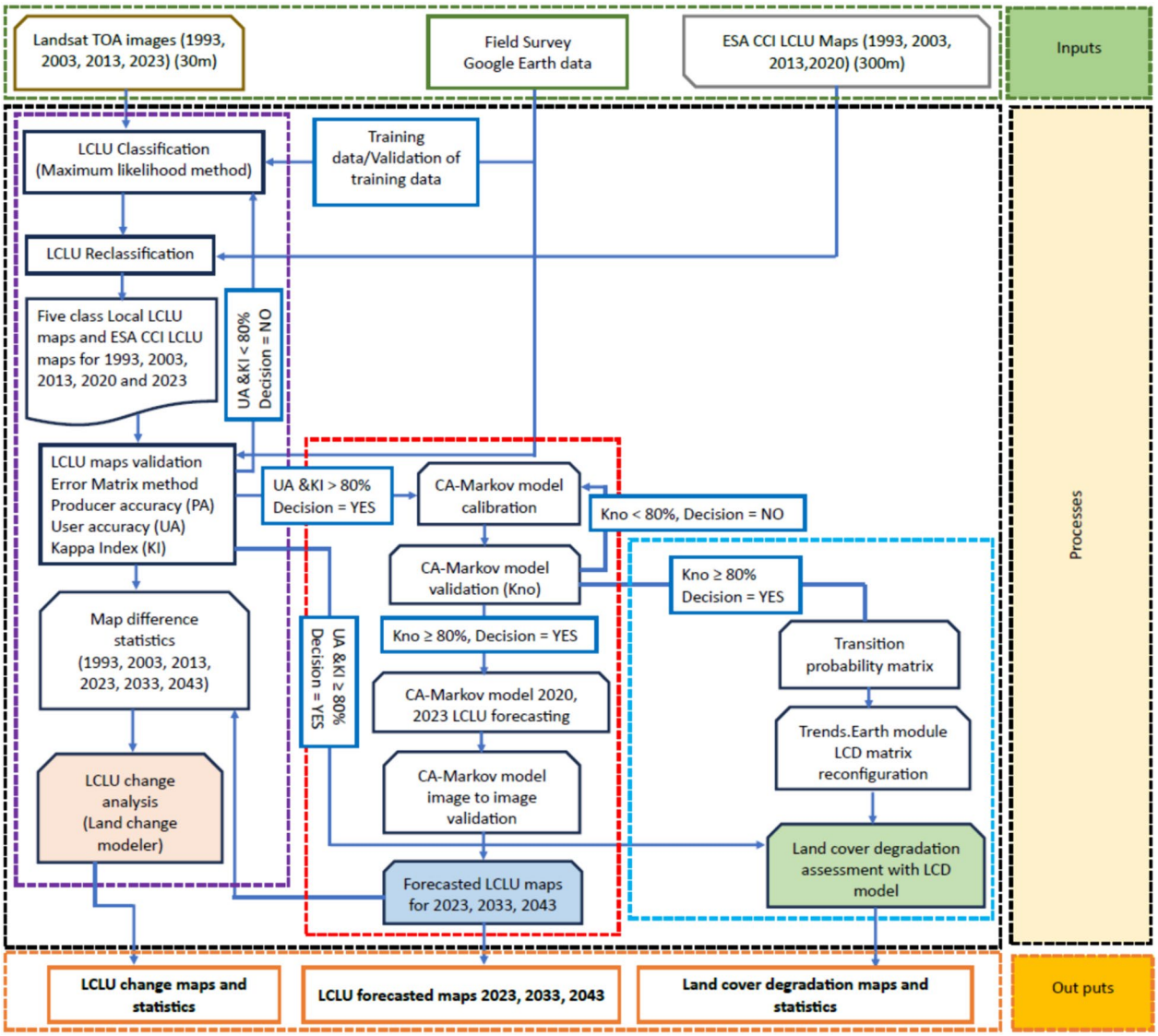

Fig. 2 Summary of the research inputs, processes and out puts in the study

representation of the same class across the image. Geographical coordinates points were collected during the reconnaissance survey using a Trimble Juno 3D Global Positioning System (DGPS) handheld device with an accuracy level of 2–5 m. These points were used to create ROIs in Google Earth Pro. The ROIs in Google Earth Pro were then converted to a ROI shapefile, which was used to generate spectral signatures in Idris Selva 17. The specific bands used for the spectral signatures depended on the sensor. For Landsat 5TM, Bands 2, 3, 4, 5, and 7 were employed, while for Landsat 8 OLI-TIRS and Landsat 9 OLI-TIRS, Bands 3, 4, 5, 6, and 7 were used. Before conducting the classification, statistics were generated to determine spectral separability. The Jeffreys-Matusita (JM) distance and the transformed divergence (TD) (Sen et al. 2019; Padma and Sanjeevi 2014; Swain and King 1973) signature separation statistics were used to identify the best band combination for LCLU classification. ROIs and band combinations with separability statistics exceeding 1.9 (JM) and 1950 (TD) were utilised for classification purposes. The bands with the highest spectral signature separability were Bands 2, 3, 4, 5, and 7 for Landsat 5TM and Bands 3, 4, 5, 6, and 7 for Landsat 8 OLI-TIRS and Landsat 9 OLI-TIRS.

Reclassifying and resampling of LCLU maps

The reclassification tool in Idris Selva was employed, in conjunction with expert knowledge and field

observations, to reclassify the seven-class global ESA Climate Change Initiative (CCI) LCLU and local LCLU maps into five classes. This process involved merging similar classes, such as grassland and wetland, and excluding the 'other class', which was not present in the global ESA dataset for the UZB. The reclassified UZB local LCLU maps, now comprising of five classes, were then resampled to the global ESA CCI LCLU spatial resolution using the nearest neighbour method in the resampling tool, resulting in a spatial resolution of 300 m. The purpose of this resampling was to standardise the local LCLU maps with the spatial resolution of the global ESA CCI datasets for performance comparison. Following the methodology explained in Sect. "Accuracy assessment of LCLU classification maps", the reclassified global ESA CCI and local LCLU maps underwent validation.

Accuracy assessment of LCLU classification maps

The stratified random sampling is a widely used method for estimating the number of sampling points required to validate a land cover and land use (LCLU) map (García-Álvarez et al. 2022; Olofsson et al. 2014; Strahler et al. 2006). The stratified approach was employed to ensure that the generated sampling points are evenly distributed across the UZB. The sample size was calculated using Eq. 1. Validation points for the LCLU maps of 1993, 2003, 2013, 2020, and 2023 were generated in ArcGIS 10.7.

$$n = \frac{z^2 O(1-O)}{d^2} \tag{1}$$

where n is the number of sampling sites, O is the anticipated user accuracy (80% in the case of this study), z is the percentile from the standard normal distribution (z = 1.96 for a 95% confidence interval); and d is the desired half-width of the confidence interval of O. The error matrix method (Olofsson et al. 2014) was utilised to calculate the accuracy statistics in ArcGIS 10.7. Each class consisted of more than 50 validation points, resulting in a total of over 900 validation points for each LCLU classification. The classifications were validated using a combination of Google Earth Pro and field data. The accuracy statistics included the producer accuracy (PA), user accuracy (UA), overall accuracy (OA), and the Kappa index (KI) (Olofsson et al. 2014; Ahmad and Quegan 2012). Only classifications with PA, UA, OA, and KI values above 0.8 were deemed acceptable, indicating a strong agreement between the LCLU classification and the actual ground status (Olofsson et al. 2014).

Dynamic LCLU simulations with the CA-Markov approach

Many researchers have used the combination of the CA–Markov model to forecast land cover and land use (Abdulrahman and Ameen 2020; Mondal et al. 2019; Hamad et al. 2018; Liping et al. 2018; Sang et al. 2011). The CA-Markov is a hybrid model that combines two different concepts: the Cellular Automata (CA) and the Markov chain. Markov Chain analysis is commonly used to simulate complex processes by studying the probabilities of transitioning between different states. This analysis is based on a discrete and random process, both in terms of time and state. The simulation model generates a transfer matrix for land cover and land use areas and a probability transfer matrix to predict trends in land use changes. The state transition probability matrix of a Markov chain determines the likelihood of a cell or pixel moving from one land use category to another. The matrix is generated by cross-tabulating two images, adjusted for proportional errors (Berto and Jacopo, 2023; Singh et al. 2015 and Memarian et al. 2012). In the Markov chain model, states are represented as $S = \{S_0, S_1, S_2, \ldots, S_n\}$. Assuming the current state is S_t, it then transitions to state S_j in the next step with a probability represented by the transition probabilitiesP_{ij}. The Markov chain model is described as in Eqs. 2 and 3 (Wang et al. 2020; Gashaw et al. 2017; Singh et al. 2015; Memarian et al. 2012).

$$S_t = P_{ij} * S_t - 1 \tag{2}$$

$$P = P_{ij} = \begin{bmatrix} P_{11} & P_{12} & P_{1n} \\ P_{21} & P_{22} & P_{2n} \\ P_{n1} & P_{n2} & P_{nn} \end{bmatrix}, \sum_{i=1}^{n} P_{ij} = 1 \tag{3}$$

where P is the matrix of Markov transitions, (i and j) are the categories of LCLU for initial and successive timeframes, respectively, n is the number of LCU classes, and P_{ij} is the likelihood that a given type of land surface will transition from one LCLU type to another.The Markov chain model has a limitation in that it operates independently of the neighbouring states of the observed cell, thus neglecting the spatial distribution of each category. As a result, while it can accurately forecast the magnitude of change, it fails to determine the appropriate direction. To overcome this limitation and gain insights into both the magnitude and direction of change, the Cellular Automata model is introduced. This model has the ability to assess the spatial characteristics of the data, thereby addressing the spatial distribution limitation of the Markov chain model. The CA aspect of the model is based on the proximity concept, where regions closer to existing areas of the same class are more likely to change to a different class, following Markov transition rules and adjacent neighbours (Berto and Jacopo 2023; Singh et al. 2015; Memarian et al. 2012). The CA model is described as in Eq. 4.

$$S_{(t-1,t)} = f\left(S_{(t-1)}, N\right) \quad (4)$$

where S is the set of finite and separate cellular states, $t-1$ denotes the various times, f is the rule for transforming cellular states in local space and N is the cellular field. The assumption made with the CA–Markov model is that if the state of a system at an earlier time is known, the probability of it being in a certain state at a later time can be determine. By using the probabilities obtained from past changes, predictions can be made about future changes (Berto and Tagliabue 2023; Singh et al. 2015; Memarian et al. 2012). Therefore, the CA–Markov model predicts both the trend and spatial structure of various LCLU categories (Wang et al. 2020; Gashaw et al. 2017; Singh et al. 2015; Memarian et al. 2012).

Calibration and validation of the CA–Markov model

Calibration and validation of the CA–Markov model are important stages in the forecasting process. The usefulness of the CA–Markov model is dependent on the results of the validation (Nyatuame et al. 2023; Mondal et al. 2016; Memarian et al. 2012).To calibrate the CA-Markov to predict the 2023 LCLU map the 2003 and 2013 LCLU classifications were used. First, the transition probabilities were generated using the Markov's Markovarian transition area estimator. Using local knowledge of the study area and the transition probabilities estimated with the Markovarian transition estimator a 5 by 5 digital filter and reclass file were generated based on the 2013 LCLU classification as the base year from which to predict the 2023 LCLU map. Using the Cellular Automata module with the 5 by 5 filter, reclass files and the 2013 LCLU map as inputs, and an iteration of 10, based on the number of years (time step) between the base year and the forecasted year, suitability maps were generated. Finally, the CA–Markov model was executed with the 2013 LCLU map as the image from which 2023 LCLU was to be predicted, Markov transition areas file and the suitability image outputted from CA module as inputs. The reader can refer to Nyatuame et al. (2023), Mondal et al. (2016) and Memarian et al. (2012) on the calibration process for the CA–Markov model.The image-to-image validation tool in Idris Selva was utilised to compare the CA–Markov model predicted 2023 LCLU map with the actual 2023 LCLU classification. The validation module assesses the level of agreement and disagreement between the CA-Markov predicted LCLU map and the classified LCLU map. An overall agreement (Kno) exceeding 0.8 indicates a strong agreement between the CA-Markov predicted and the classified LCLU maps (Nyatuame et al. 2023; Mishra et al. 2018; Mondal et al. 2016). In this study, if the overall accuracy assessment of the LCLU classification was above 85%, and the CA-Markov predicted LCLU did not achieve an overall accuracy of 0.8, the LCLU maps were not reworked. Instead, multiple reclass files were attempted until the desired accuracy result of over 80% for the CA-Markov predicted LCLU map was achieved.

Forecasts of the 2033 and 2043 LCLU maps

The forecasts for the 2033 and 2043 LCLU maps were conducted using the validated CA–Markov model. This model utilized the Markov transition areas file and the suitability image generated from the calibration of the CA module, which exhibited an overall agreement (Kno) of the predictions above 0.8 (Mondal et al. 2016). The base years for these predictions were 2023 and 2033, respectively.

LCLU change assessment with the Land Cover Modeler

To assess the changes in the LCLU between time steps the land cover modeler in Idris Selva was used. The change analysis involved the gains and losses of each LCLU class, net change by each class and the contributors to the net change in each class.

Configuring of the LCD matrix and LCD analysis

To align with the validated five class local LCLU maps and the global ESA CCI LCLU maps the Land cover degradation matrix in Trends.Earth module was first reconfigured to five classes from seven classes configuration. Each LCLU class was assigned an identification (ID) number from 1 to 5, with no data assigned zero (0) as the ID. The typological table (Table 1) in the Trends.Earth land cover degradation module was then manually configured using the local knowledge of LCLU transitions in the study area, the information obtained from the transition probability matrices during CA–Markov model calibration in Idris Selva and the transition information in Trends.Earth module. Each transition was assigned a category as follows; the transitions corresponding to degradation (− sign), improvement (+ sign), or stable (no change in terms of land condition) (zero) (Table 1). Since the Trends.Earth module does not go beyond the year 2030 the LCLU maps false labels were used going back 20 years with 1973, 1983, 1993, 2003, 2013, 2023 in place of 1993, 2003, 2013, 2023, 2033 and 2043 respectively.

Results and discussion

Local Landsat-based LCLU maps and the Global ESA CCI LCLU maps

Landsat data were successfully used to assess the LCLU for the UZB (Fig. 3). The changes in the spatial distribution of LCLU are more visible in the local maps than the global ESA CCI LCLU maps (Fig. 3). The differences in the LCLU between the local maps and the global ESA

Table 1 Reconfiguration of the land cover degradation matrix in Trends. Earth

Land cover in initial year	Land cover in target year: Forest	Grassland	Cropland	Built up/Bareland	Water
Forest	0	-	-	-	-
Grassland	+	0	-	-	-
Cropland	+	+	0	-	-
Built up/Bareland	+	+	+	0	-
Water	-	-	-	-	0

Legend	Degradation	Stable	Improved
	-	0	+

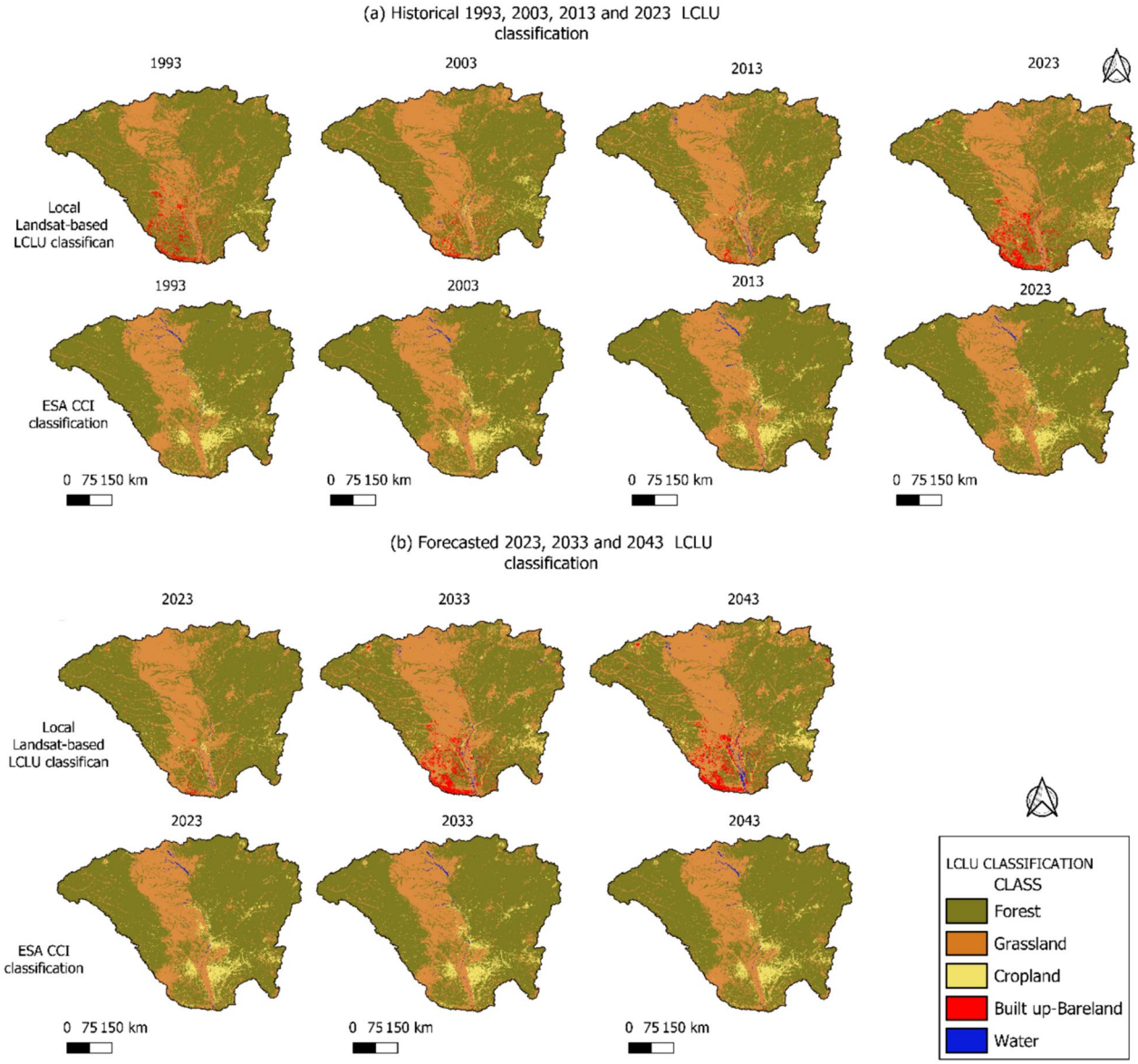

Fig. 3 **a** Historical Landsat-based local LCLU classifications and global ESA CCI LCLU classifications for the years 1993, 2003, 2013, 2023 and **b** the CA-Markov based predictions for 2023, 2033 and 2043 with Landsat-based LCLU maps and global ESA CCI maps in the Upper Zambezi Basin, southern Africa

CCI LCLU maps could be attributed to the differences in the spatial resolutions of the classifications (Local Landsat-based LCLU maps with 30 m spatial resolution and ESA CCI LCLU at 300 m spatial resolution) and the reliability of the training data used in the classifications (Duarte et al. 2023; Friedl et al. 2022; Tulbure et al. 2022; Wang et al. 2019).

Accuracy assessment of LCLU classifications

In thematic mapping using remotely sensed data, accuracy is the term commonly employed to denote the degree of correctness of the map or classification (Foody 2002). Accuracy refers to the level of agreement of the classification with the real-world data. Accuracy assessment serves to establish the level of confidence in the classification(s) (Islami et al. 2022; Rwanga and Ndambuki 2017; Bogoliubova and Tymków 2014; Foody 2002) prior to its application for a specific purpose.

Accuracy assessment of local LCLU maps and the Global ESA CCI LCLU maps

The accuracy assessment for historical classification relied on field surveys, Google Earth data, and the confusion matrix approach. The stratified sampling approach with a total of 915 sampling points was used. Four metrics were utilized: producer accuracy (Fig. 4a, d and Tables A1 & A2 in the appendices), user accuracy (Fig. 4b, e and Tables A1 & A2 in the appendices), overall accuracy and kappa index (Fig. 4c, f and Tables A1 & A2 in the appendices). Generally, over the years, both the local-level Landsat-based LCLU maps and the ESA CCI LCLU maps demonstrated strong accuracy, with Overall accuracy/Kappa coefficients exceeding 0.9 (Tables A1 & A2 in the appendices). The producer accuracy and the user accuracy for each class were also notably high, generally surpassing 80% (Tables A1 & A2 in the appendices). For the locally classified LCLU maps, greater uncertainty was observed in estimating the PA and UA metrics for the cropland and water classes (Fig. 4a, b). In the ESA CCI LCLU maps, greater uncertainty was observed in the cropland, build up/bareland, and water classes (Fig. 4d, e). When compared to the local Landsat-based LCLU classification, the ESA CCI LCLU classification showed lower user accuracy values (Tables A1 & A2 in the appendices) and greater uncertainty (Fig. 4) for the cropland and build up/bareland classes. Overall, the locally produced Landsat-based LCLU maps demonstrated greater accuracy than the global ESA CCI LCLU maps.

Validation of the CA–Markov model

For future projected maps, accuracy metrics for image-to-image comparison; Kstandard, Kno, Klocation, and Klocation strata, in Idris Selva were employed. Kno indicates the overall agreement. Klocation indicates the extent to which the two maps agree in terms of location of each category. Kquantity indicates the extent to which the two maps agree in terms of quantity of each category (Mondal et al. 2016). According to Cohen's

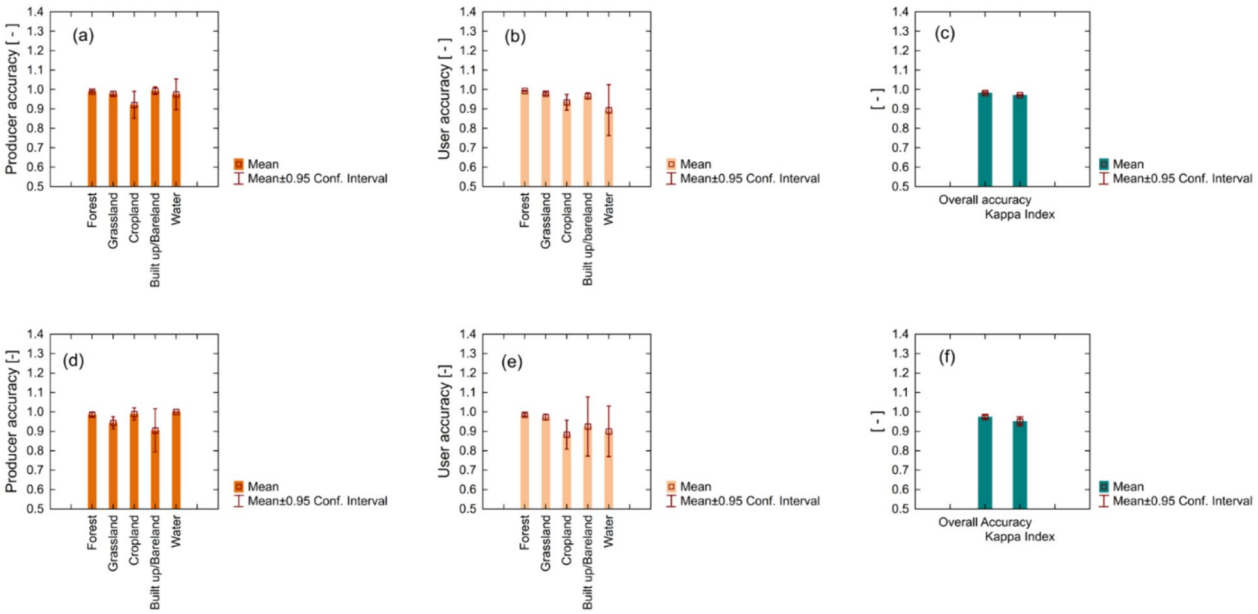

Fig. 4 Accuracy assessment metrics for local Landsat-based LCLU classification and ESA CCI LCLU classification **a, d** producer accuracy, **b, e** user accuracy and overall accuracy and Kappa Index **c, f** respectively

Kappa coefficient of agreement interpretation (Cohen, 1960), a range of 0.6–0.79 indicates moderate agreement, 0.80–0.90 indicates strong agreement, while values above 0.90 indicate almost perfect agreement. An overall accuracy agreement of 80% is recommended (Mondal et al. 2016; Foody 2002; Anderson et al. 1976). The CA–Markov model showed strong overall agreement (Kno) of above 0.85 in both scenarios with the local LCLU maps (Table 2) and global ESA CCI LCLU maps (Table 3). The CA–Markov was then used to make the 2023, 2033 and 2043 predictions with the 2013, 2023 and 2033 (local LCLU maps and global ESA CCI LCLU maps) as base years for the predictions.

Agreement between local LCLU maps and the Global ESA CCI LULC maps

The local LCLU maps demonstrated higher user accuracy values and an overall kappa index of agreement (KIA) compared to the global ESA CCI LCLU maps (Fig. 4 and Tables A1 and A2 in the appendices). Consequently, the local maps were employed as the reference images for evaluating the similarity between the local LCLU classifications and global ESA CCI LCLU classifications using the cross-tabulation method. Despite similarities observed visually between the local LCLU maps and the ESA LCLU maps, the cross-tabulation analysis presents a different perspective, indicating weak agreement between the classifications. In general, the forest class exhibited the highest KIA between the local LCLU maps and global ESA CCI LCLU maps over the years, ranging from 0.739 to 0.910 (Table 4). The grassland class displayed a KIA ranging from 0.158 to 0.589, while the cropland class exhibited a KIA ranging from 0.153 to 0.234. The built-up/bare land class demonstrated the lowest KIA among the classes, ranging from 0.003 to 0.008. The water class had a KIA ranging from 0.175 to 0.391. Cramer's V ranged from 0.445 to 0.560, indicating an agreement level of generally less than 60% between the local LCLU maps and the global ESA CCI LCLU maps. The significant disparities between the local LCLU maps and the global ESA CCI LCLU maps appear primarily in the grassland, cropland, built-up/bare land, and water classes (Table 4). These distinctions underscore the importance of leveraging local knowledge of the study area and the necessity of locally generated LCLU maps.

Table 2 Validation of the 2023 predicted LCLU map using the CA–Markov model configured with 2003 and 2013 local Landsat data-based LCLU maps

Classification agreement/disagreement According to ability to specify accurately quantity and allocation			
	Information of quantity		
Information of Allocation	No[n]	Medium[m]	Perfect[p]
Perfect [P(x)]	P(n) = 0.5446	P(n) = 0.9797	P(n) = 1.0000
Perfect Stratum [K(x)]	K(n) = 0.5446	K(n) = 0.9797	K(n) = 1.0000
Medium Grid [M(x)]	M(n) = 0.4784	M(n) = 0.8762	M(n) = 0.8792
Medium Stratum [H(x)]	H(n) = 0.1667	H(n) = 0.3241	H(n) = 0.3224
No [N(x)]	N(n) = 0.1667	N(n) = 0.3241	N(n) = 0.3224
Agreement Chance	= 0.1667		
Agreement Quantity	= 0.1575		
Agreement Strata	= 0.0000		
Agreement Gridcell	= 0.5521		
Disagree Gridcell	= 0.1035		
Disagree Strata	= 0.0000		
Disagree Quantity	= 0.0203		
Kno	0.8514		
Klocation	0.8422		
Klocation Strata	0.8422		
Kstandard	0.8168		

Table 3 Validation of the 2020 predicted LCLU map using the CA–Markov model configured with 2003 and 2013 global ESA CCI LCLU maps

Classification agreement/disagreement According to ability to specify accurately quantity and allocation			
	Information of quantity		
Information of allocation	No[n]	Medium[m]	Perfect[p]
Perfect [P(x)]	P(n) = 0.5255	P(n) = 0.9988	P(n) = 1.0000
Perfect Stratum [K(x)]	K(n) = 0.5255	K(n) = 0.9988	K(n) = 1.0000
Medium Grid [M(x)]	M(n) = 0.5236	M(n) = 0.9966	M(n) = 0.9955
Medium Stratum [H(x)]	H(n) = 0.1667	H(n) = 0.3521	H(n) = 0.3517
No [N(x)]	N(n) = 0.1667	N(n) = 0.3521	N(n) = 0.3517
Agreement Chance	= 0.1667		
Agreement Quantity	= 0.1855		
Agreement Strata	= 0.0000		
Agreement Gridcell	= 0.6444		
Disagree Gridcell	= 0.0023		
Disagree Strata	= 0.0000		
Disagree Quantity	= 0.0012		
Kno	0.9959		
Klocation	0.9965		
Klocation Strata	0.9965		
Kstandard	0.9947		

Composition and comparison of LCLU classes across years

The locally produced maps exhibit a greater level of detail and offer more nuanced temporal variations in the estimation of LCLU (Fig. 5a and Table 5), in contrast to the global product provided by ESA CCI (Fig. 5b). The LULC classifications by global ESA CCI diverge from the local LULC maps, as they depict an increase in forest cover over time and a decrease in grassland (Fig. 5b

Table 4 Similarity between local LCLU maps and global ESA CCI LCLU maps

Kappa index of agreement (KIA) per LCLU class							
Year	**Forest**	**Grassland**	**Cropland**	**Built up/bareland**	**Water**	**Over-all KIA**	**Cramer's V**
1993	0.739	0.158	0.200	0.004	0.391	0.266	0.445
2003	0.852	0.573	0.222	0.007	0.347	0.804	0.560
2013	0.829	0.589	0.234	0.008	0.318	0.810	0.556
2023	0.839	0.501	0.153	0.003	0.317	0.755	0.540
2033	0.909	0.514	0.201	0.003	0.175	0.774	0.550
2043	0.910	0.512	0.202	0.003	0.179	0.774	0.550

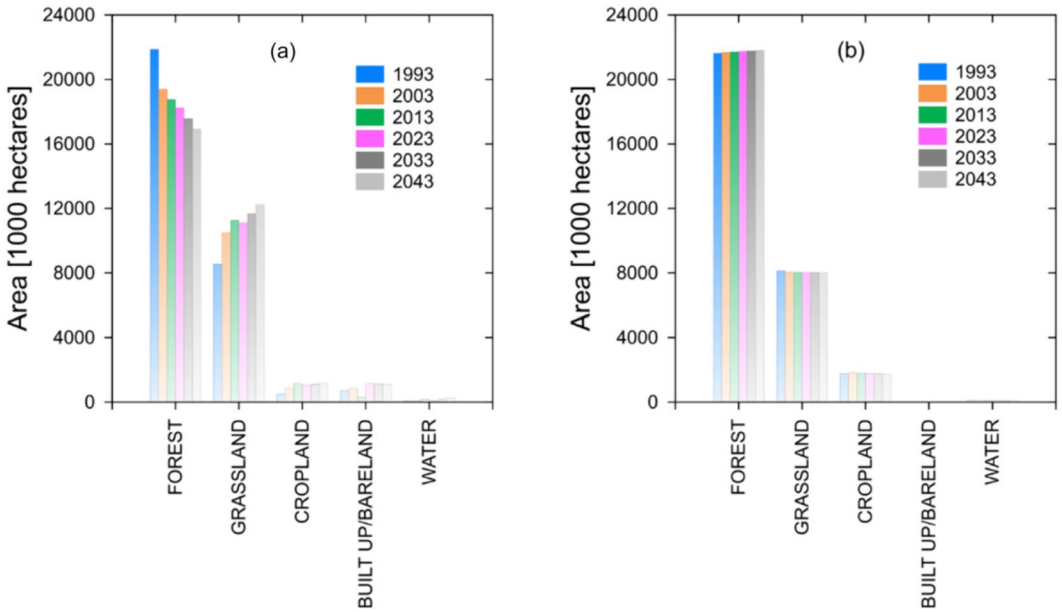

Fig. 5 Historical and future projected composition of LCLU area in the Upper Zambezi Basin across years 1993–2043: **a** Landsat-based locally classified LCLU maps and **b** global ESA CCI LCLU maps

Table 5 Percentage (%) coverage of the LCLU area from 1993 to 2043

	Local Landsat-based LULC classification						**Global ESA CCI LULC classification**					
	1993	**2003**	**2013**	**2023**	**2033**	**2043**	**1993**	**2003**	**2013**	**2023**	**2033**	**2043**
Forest	69.05	61.26	59.23	57.63	55.52	53.45	68.31	68.45	68.57	68.67	68.76	68.85
Grassland	26.98	33.11	35.62	35.07	36.84	38.61	25.68	25.45	25.38	25.34	25.30	25.26
Cropland	1.54	2.71	3.62	3.36	3.52	3.69	5.64	5.75	5.68	5.63	5.58	5.54
Built-up/bare land	2.22	2.66	0.94	3.67	3.56	3.46	0.03	0.04	0.04	0.04	0.04	0.04
Water	0.21	0.25	0.59	0.27	0.55	0.78	0.34	0.31	0.32	0.32	0.32	0.32

and Table 5). However, these global ESA CCI LCLU classifications are inconsistent with numerous studies that have demonstrated a decline in forested areas in Zambia, Angola, and southern Africa as a whole (Kissanga et al. 2024; Tiamgne et al. 2021; Mendelsohn 2019; Phiri et al. 2019; Shakachite et al. 2016).

Contrary to the ESA CCI estimates, the local LCLU classifications appear to be consistent with findings from the above cited studies that suggest a decline in forested areas, a rise in agricultural land, and the expansion of built-up or barren land in the southern African region, including specific countries like Angola and Zambia.

Nonetheless, the UZB primarily comprises forested areas, with over 50 percent of its total landmass classified as forest by 2043 (Table 5).

Change analysis of the LCLU

Gains and losses analysis

Overall, based on local classifications, it is expected that the historical changes in the LCLU of UZB will be reflected in future projections. The gains in area of cropland, grassland, and built-up/bareland are projected to exceed the losses (Fig. 6a, b). However, when it comes to forest area, the gains are expected to be lower than the losses. The overall temporal trend indicates a continued reduction in forest area, accompanied by increases in area of built-up/bareland, cropland, and grassland. These changes are not easily observable when using the global ESA CCI LCLU data (Fig. 6c, d), highlighting the need to evaluate the suitability of this product for local-level applications. Detailed change analysis for each LCLU class is provided in the proceeding sections.

Forest cover change and drivers of change

The decline in forest area during the specified period was clearly evident in the locally generated maps and aligns with the overall decreasing trend in forest cover in Angola and Zambia (Chundu et al. 2024; Kissanga et al. 2024; Banda et al. 2023; Phiri et al. 2019). From 1993 to 2003, there was a net decline in forest area of − 4.23%. Between 2003 and 2013, the forest area declined by − 1.74%, while between 2013 and 2023, there was a net decline in forest area of 4.13%. Throughout the period 1993–2023, there was a consistent decrease in the area of forest cover in the UZB. Key factors contributing to the reduction in forest area from 1993 to 2023 included the expansion of grasslands (− 5.38%), population-driven shifts leading to an increase in croplands (− 1.04%), and the growth of built-up/bare lands (− 0.5%). Forecasts predict a decrease in forest area of -1.29% and − 1.26% for the periods 2023–2033 and 2033–2043, respectively. The anticipated decline in forest cover is primarily expected to be driven by the expansion of grasslands (− 1%),

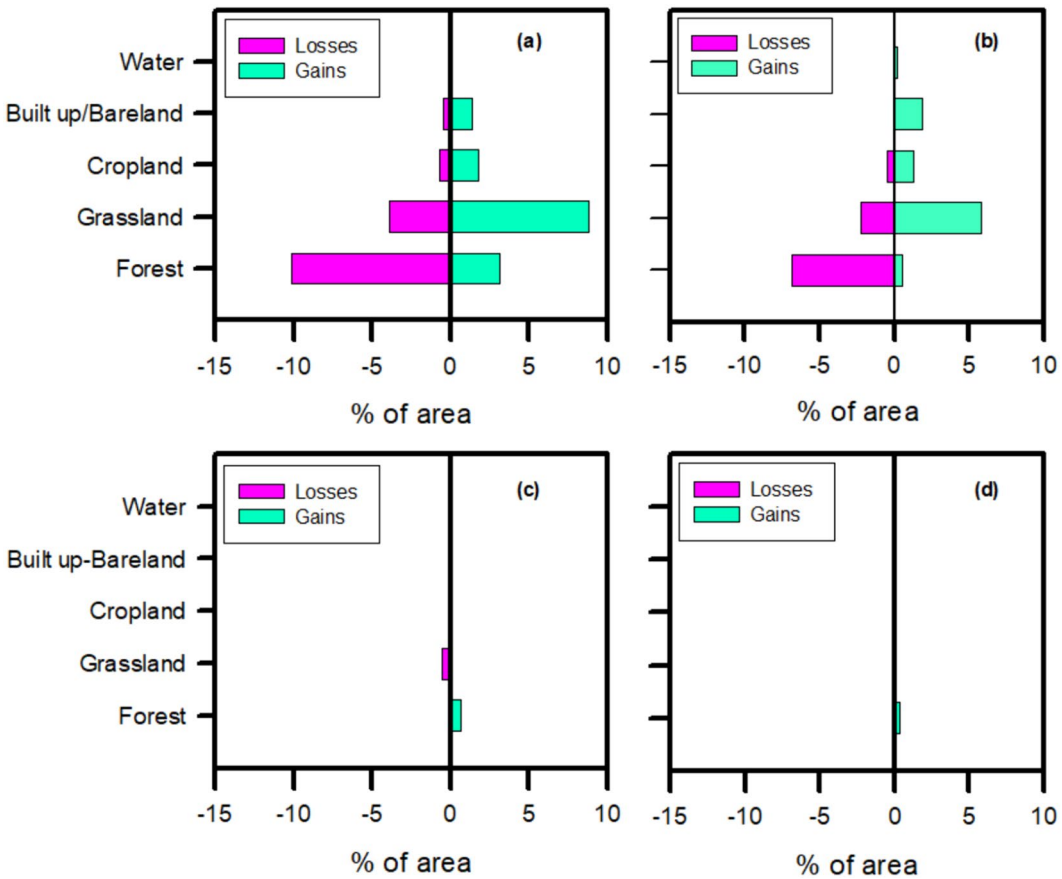

Fig. 6 Gains and losses in LCLU for the period 1993–2043 in the Upper Zambezi Basin. **a** gains and losses between 1993 and 2023, **b** gains and losses between 2023 and 2043 for local LCLU classifications. **c** gains and losses between 1993 and 2023, **d** gains and losses between 2023 and 2043 using the global ESA CCI LCLU classification

croplands (− 0.25%), and built-up areas/bare land (0.02%) (Fig. 7).

Grassland change and drivers of change

The grassland area experienced a general net increase of 3.9% between 1993 and 2003, followed by a net growth of 1.36% between 2003 and 2013. Furthermore, an observed net increase of 1.72% occurred between 2013 and 2023. Future projections indicate that the grassland area will continue to expand, with an expected net increase of 1.8% between 2023 and 2033, and a subsequent net increase of 1.08% between 2033 and 2043. From 1993 to 2023, the reduction in forest area contributed to a 5.38% increase in grassland area. Conversely, the reduction in grassland area was primarily driven by the expansion of cropland (− 0.06%), built-up area/Bareland (0.4%), and water (− 0.01%). Looking ahead to 2043, the projected increase in grassland area will follow a similar pattern, with 5.01% resulting from changes in forest area and 0.04% resulting from changes in cropland. Conversely, the projected reduction in grassland area (− 1.36%) will mainly be due to the expansion of built-up area/Bareland and conversion to water (− 0.16%) (Fig. 7).

Cropland change and drivers of change

The cropland area experienced a net increase of 0.89% between 1993 and 2003, 0.37% between 2003 and 2013, and 0.61% between 2013 and 2023. Future projections indicate a significant increase in cropland area, with a projected growth of 4.7% between 2023 and 2033, followed by a minimal increase of 0.11% between 2033 and 2043 (Fig. 7). These observations in cropland align with the findings of various studies, including those by Kissanga et al. (2024), Chundu et al. (2024), and Phiri et al. (2019), which demonstrate a consistent trend of cropland expansion in Angola and Zambia over the years.

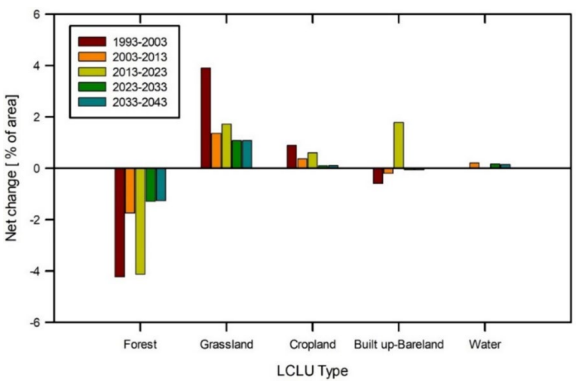

Fig. 7 Net change percentage in each of the LCLU over the assessed periods in the UZB

Built-up/Bare Land change and drivers of change

The built-up/bare land area experienced a net reduction of -0.59% between 1993 and 2003, mainly due to conversion to cropland (− 0.07%) and grassland (− 0.63%). Between 2003 and 2013, there was a further decrease of − 0.31% (Fig. 7). However, between 2013 and 2023, there was a net increase of 1.79% in the built-up/bare land area, driven by the conversion of forest area (0.33%), grassland (1.4%), and cropland (0.06%). Looking ahead, it is projected that between 2023 and 2033, the built-up/bare land area will reduce by -0.06% due to the conversion to cropland (− 0.13%), while experiencing an increase from the conversion of forest cover (0.04%) and grassland (0.03%) (Fig. 6). Similarly, the future projections for the period 2033–2043 indicate a net reduction of − 0.06% in the built-up/bare land area due to the conversion to grassland (− 0.12%), while gains will come from the conversion of forest area (0.02%) and cropland (0.04%).

Water body change and drivers of change

This is one of the most significant classes in the UZB with implications on the health of various ecosystems, including wetlands. Between 1993 and 2023 the net change in the area covered by water in the UZB was 0.04% indicating a net increase of about 190 km^2. The change was mainly due to conversion of forest area to water (0.03%) and grassland to water (0.01%). Between the period 2023 and 2043 the projection is that area covered by water will increase by a net of 0.19% (Fig. 7) which is 962 km^2. Main contributors to this change are conversion from grassland to water body (0.16%) and conversion from forest cover to water body (0.02%).

Transitions in LCLU and land cover degradation

Transitions in LCLU

The primary LCLU transitions observed between 1993 and 2023 were the conversion of forest cover to grassland and cropland. Approximately 42,000 km^2 of forest were transformed into grassland, while about 7000 km^2 were converted to cropland (Figs. 8a and 9a). In both Angola and Zambia, where the UZB is located, the causes of forest-to-grassland conversion can be attributed to factors such as bush fires, timber harvesting, and charcoal burning for energy needs in both rural and urban areas (Chundu et al. 2024; Kissanga et al. 2024; Phiri et al. 2019). Moreover, the increase in anthropogenic factors, such as population growth, has resulted in a higher demand for food, leading to the expansion of cropland and settlements, which encroach upon forested areas, as shown in Fig. 8a (Kissanga et al. 2024; Phiri et al. 2019). Grassland, on the other hand, has predominantly transitioned to forest cover (14,000 km^2) and built-up/bareland

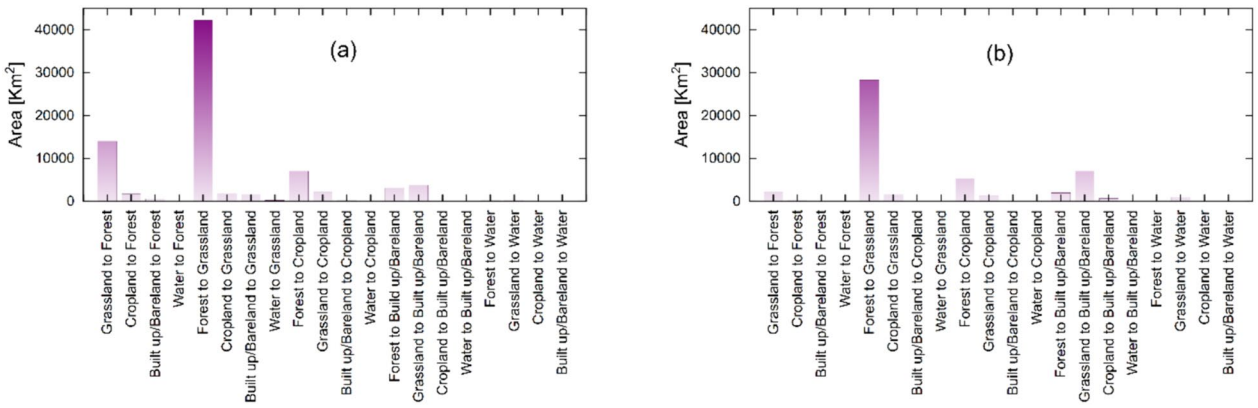

Fig. 8 Illustration of the historical and forecasted temporal transitions of LCLU classes in the Upper Zambezi Basin over two periods: **a** spanning from 1993 to 2023, represents the historical data, while (**b**), spanning from 2023 to 2043, represents the forecasted data using the local Landsat-based LCLU maps

(3700 km^2). Conversely, portions of cropland have transitioned to grassland (1800 km^2), as have areas of built-up/bareland (1600 km^2) (Figs. 8a and 9a). The forecasted LCLU transitions for the period between 2023 and 2043 are expected to follow a similar pattern in the UZB (Figs. 8b and 9b), with forest cover mostly converting to grassland, cropland, and built-up/bareland. Grassland is expected to primarily transition to forest (2200 km^2) and built-up/bareland (7000 km^2) (Figs. 8b and 9b).

Spatial and temporal distribution of land cover degradation

Land cover degradation in the UZB seems to be widespread throughout the study area (Fig. 10). Between 1993 and 2023, the most significant degradation occurred in the forest cover, primarily due to the conversion of forests into croplands, the development of human settlements, and the conversion to grasslands. The degradation of grasslands was mainly caused by the conversion of grasslands into croplands and built-up/bare lands. The largest land cover degradation occurred between 1993 and 2003, with approximately 47,165 km^2 degraded, accounting for 15% of the total UZB catchment area. Similarly, between 2013 and 2023, the total degraded area was approximately 43,830 km^2, representing about 14% of the UZB catchment area (Fig. 11). The most significant improvement in land use and land cover was observed between 2003 and 2013. The period from 2023 to 2033 is projected to have approximately 27,754 km^2 (8% of the total UZB catchment area) as degraded land, primarily due to the anticipated ongoing conversion of forest cover into grasslands, croplands, and built-up/bare lands. However, the degraded land cover is projected to decrease in the period from 2033 to 2043 compared to the period from 2023 to 2033 (Fig. 11).

Land cover degradation was observed throughout the entire spatial extent of the UZB, both in historical and projected periods (Fig. 9). Phiri et al. (2019) identified various driving factors that contribute to long-term changes in land cover in Zambia.

These factors include the percentage of agricultural area, proximity to water bodies, changes in crop yield, average temperature, and elevation. Significant factors influencing the loss of forest cover include human population density, crop yield per hectare, and mean crop yield. The observed land cover degradation in the UZB corresponds to the findings of Phiri et al. (2019), as the degradation is evident near human settlements, water bodies, and croplands (Figs. 3 and 10). Overlaying wetlands on the maps displaying the spatial distribution of land cover degradation in the UZB reveals degradation in and around all wetlands, primarily due to the conversion of grasslands into woody vegetation (i.e., forest) and croplands (Fig. 7a). These observations highlight the threat posed to wetland ecosystems by changes in LULC in wetlands and in the wetland catchments.

Discussion

Differences in agreement between LCLU classes

In comparison to the global ESA CCI LCLU, the locally generated Landsat-based LCLU maps demonstrated superior accuracy in terms of user accuracy and overall kappa index results. Overall, the proportional area comparison showed over 75% agreement between global ESA CCI LCLU and local Landsat-based LCLU, except for the year 1993 which showed less than 50% agreement. The disparity between the global ESA CCI LCLU maps and the local LCLU maps varied depending on the land cover and land use classes. Dominant LCLU classes, forest cover and grassland, generally showed significant

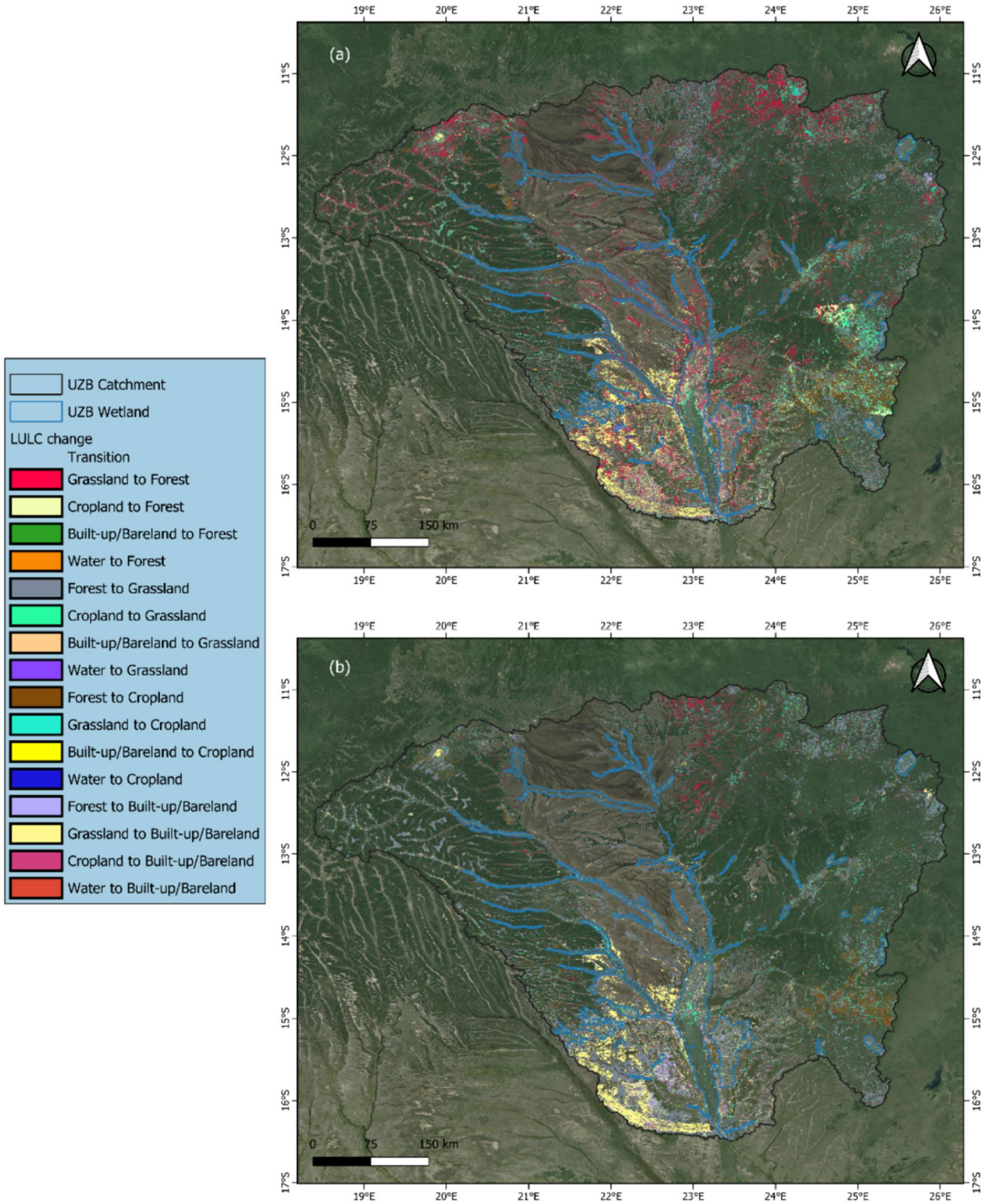

Fig. 9 An overlay of UZB wetlands on the Google Earth image and the local Landsat-based LCLU spatial transition maps for the period **a** 1993–2023 and **b** 2023–2043

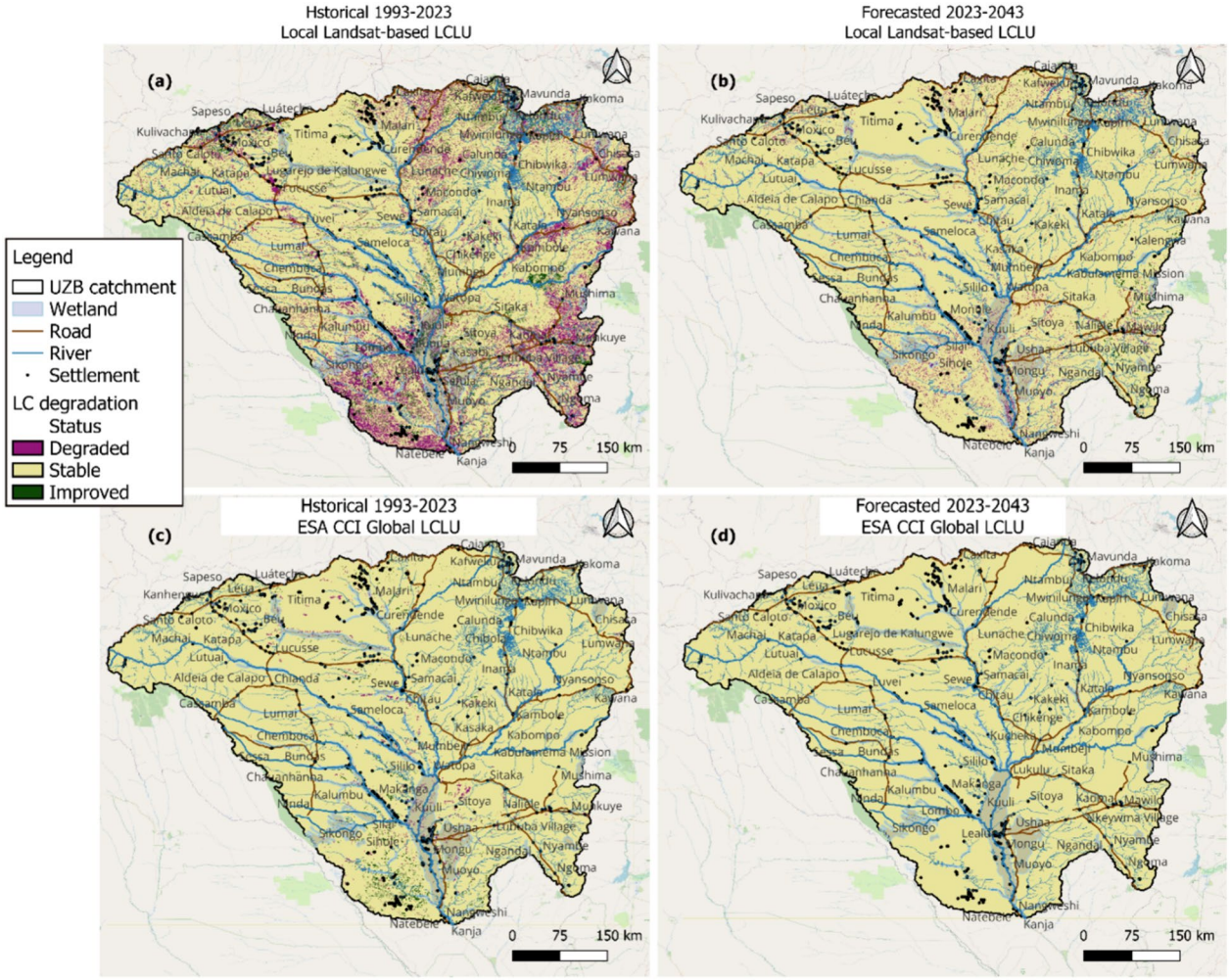

Fig. 10 Trends.Earth module assessment of land cover degradation in the UZB; based on locally classified LCLU maps **a** 1993–2023, **b** 2023–2043 and the global ESA CCI LCLU maps **c** 1993–2023 and **d** 2023–2043. The OpenStreet Map is used as the background

agreement, KIA > 80%; 50% respectively (Table 4). However, there was less concurrence observed in smaller LCLU classes, such as cropland, settlement, and water bodies. For instance, Bayas et al. (2017) found that global ESA CCI overestimated cropland. Other studies have shown similar results in which global ESA CCI LCLU showed good agreement proportional to the area of each LCLU class (Reinhart et al. 2021).

An accuracy assessment of the global ESA CCI 20 m land cover product conducted in Gabon, Ivory Coast, Kenya and South Africa showed mixed performance (Lesiv et al. 2019). Lesiv et al. (2019) found overall accuracy of between 44% (South Africa) and 91% (Gabon). They also showed that user accuracy increased by merging certain classes. Both Reinhart et al. (2021) and Lesiv et al. (2019) attributed the errors in global ESA CCI LCLU to misclassification of the classes due to the training data utilised in the classification process. In this study, it was observed that the ESA CCI LCLU misclassified significant areas of built-up land and forests as cropland. Additionally, in some instances, large grassland areas were erroneously classified as forest cover. This misclassification can likely be attributed to the training data utilised in the classification process of the global ESA CCI LCLU product, similar to the findings of Reinhart et al. (2021) and Lesiv et al. (2019). The 300-m spatial resolution in global ESA's LCLU data may cause errors resulting in underestimation/overestimation of LCLU classes due to mixed pixels. Mixed pixels occur when a single pixel represents multiple land cover types, making it challenging to accurately classify the pixel's true identity (Lillesand et al. 2015).

Drivers of changes in land cover and land use

Although this study did not evaluate the underlying factors driving the alterations in land cover and land use,

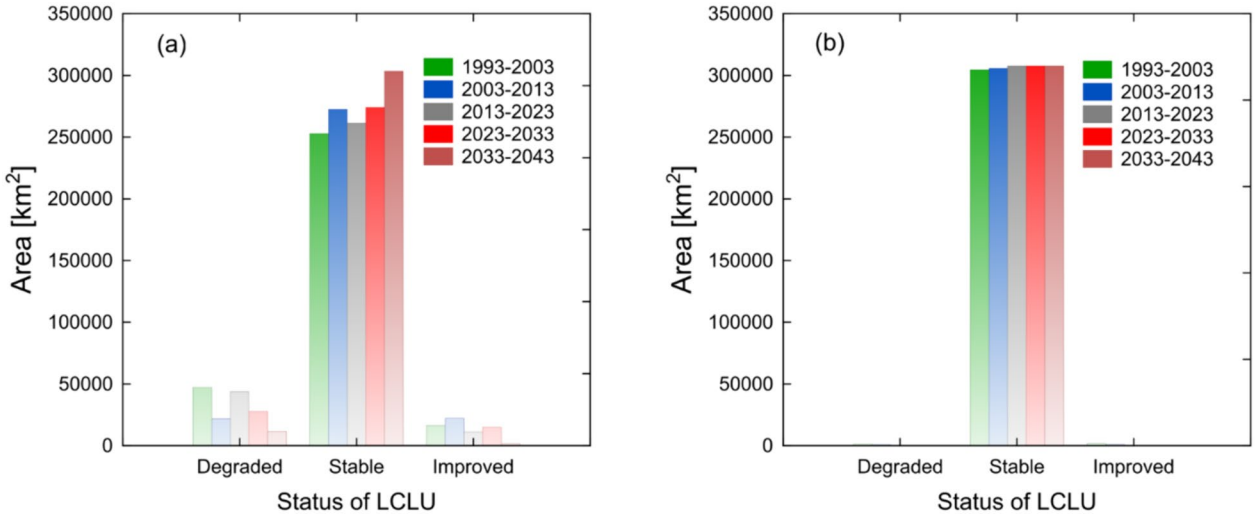

Fig. 11 Trends.Earth module assessment of the temporal magnitude of land cover degradation in the UZB **a** generated using locally Landsat-based LCLU maps, and **b** generated using the global ESA CCI LCLU maps

previous studies conducted in Zambia (Phiri et al. 2019), Angola (Kissanga et al. 2024), the wider African continent (Assede et al. 2023; Kleemann et al. 2017; Kindu et al. 2015) as well as other regions worldwide (Kim et al. 2014), have elucidated these drivers. The major drivers include: an increase in population, distance to facilities (road network, rivers, railways), economic status of rural households, changes in agricultural practices, climate variables, topography and many more. According to a review of the drivers of changes in LCLU in Africa, Assede et al. (2023) found that agriculture dominates natural forest conversions. They also found that natural vegetation is largely converted to arable land and settlements, leading to unprecedented accelerated soil erosion and land degradation. These observations align with the findings of this study, which show that forests were typically converted to grassland, cropland and settlements as explained in Sect. "Change analysis of the LCLU". Assede et al. (2023) further revealed that the observed loss in forest areas is mainly associated with fringe population growth and the associated demand for firewood, charcoal, and construction materials. These findings align with the observations made by Kissanga et al. (2024) in Angola and in Zambia by Phiri et al. (2019). However, charcoal production and firewood collection are short-term changes that can be reversed over time through woodland recovery, unless these areas are converted into commercial agriculture (Assede et al. 2023). It is crucial to consider the resilience of woodlands in this context. Zambezian woodlands are known for their ability to regrow strongly after tree harvesting (Phiri et al. 2019). This may explain the gains in forest cover for the period 1993–2023 (Fig. 6a).Mwampamba et al. (2016) showed that grasslands in Africa are reducing rapidly due to conversion to arable land. This observation aligns with the findings of this study which shows that the reduction in grassland area was primarily driven by the expansion of cropland (− 0.06%) and built-up area/Bareland (− 0.4%).

Implications of the land cover degradation

Land cover degradation is a significant environmental problem with extensive policy implications. It involves the permanent loss of natural vegetation due to various factors such as deforestation, urbanization, and agriculture (Kouassi et al. 2021; Herrmann et al. 2020). This degradation has a profound impact on the environment. For instance, land cover degradation results in the destruction of natural habitats, leading to a decline in biodiversity (Baidoo et al. 2023; Maitima et al. 2009). This, in turn, has a domino effect on the entire ecosystem, as the loss of one species can affect the survival of others. Land cover degradation contributes to climate change by releasing carbon dioxide into the atmosphere (Barati et al. 2023). Trees and other plants absorb carbon dioxide as part of photosynthesis, so when they are removed, this carbon is released back into the atmosphere. Land cover degradation can lead to soil erosion, resulting in the loss of topsoil due to wind or water. This can damage soil fertility and reduce agricultural productivity (Ferreira et al. 2022; Gebresamuel et al. 2010). Land cover degradation can lead to changes in hydro-morphology, flow volumes and water pollution by allowing sediment and nutrients from eroded soil to enter waterways. This contamination can harm aquatic ecosystems and contaminate drinking

water supplies (Kayitesi et al. 2022; Näschen et al. 2019). These implications must be viewed within the context of the limitations of the study as highlighted below.

Limitations of LCLU forecasts using CA-Markov

The limitations of the CA–Markov model have been reviewed by Ghosh et al. (2017) and particularly noted by Asif et al. (2023), Sang et al. (2011), Kamusoko et al. (2009). Some of the limitations of the CA–Markov model include:

Inaccurate simulations

In this study, the simulations did not consider external variables such as the effects of government policies, socio-economic interactions, and other environmental drivers. As a result, changes in land cover and land use may not have been accurately simulated, leading to discrepancies between predicted and observed changes (Ghosh et al. 2017). This may be attributed to the complex interactions between social, economic, and environmental drivers. However, the simulations in this study showed good agreement with the actual observations, indicating minimal errors and suggesting that the study is acceptable for use.

Limited temporal scope

CA-Markov models typically rely on short-term historical data, such as the 10-year periods used in this study. However, this approach may not capture long-term trends or future uncertainties, which can limit their ability to accurately predict future land use changes (Ghosh et al. 2017). This could explain the reduction in the forecasted land degradation for the UZB. It is possible that the actual future land degradation will be higher than what the study has forecasted.

Static transition probabilities

CA-Markov models assume that transition probabilities between land use types remain constant over time. However, these probabilities may change due to various factors, such as policy changes or technological advancements (Ghosh et al. 2017). In view of this limitation the LCLU and land degradation forecasts made using the CA-Markov approach in this study may not be very accurate as policy changes and technological advancements have not been considered in the simulations.

Policy considerations

The Upper Zambezi Basin is home to the source of the Zambezi River and has diverse ecosystems. These ecosystems support livelihoods in Angola and Zambia. One such ecosystem is the Barotse wetlands in Zambia, designated as a Ramsar site (Beilfuss 2012; Fanshawe et al. 2010; Timberlake 2000). Land degradation in the Upper Zambezi Basin can affect the Lower Zambezi's ecosystems, hydro-power generation, and agriculture. Given the significant environmental impacts of land cover degradation, it is important for policymakers to take action to address this issue.

Policymakers can protect and restore natural habitats by implementing conservation measures, such as creating protected areas and reforestation programs. Policymakers can promote sustainable agriculture by providing incentives for farmers to adopt climate smart agriculture practices and those practices that minimize land degradation, such as crop rotation and contour ploughing. Policymakers can reduce deforestation by implementing policies that discourage the clearing of forests, such as taxes on logging and land use regulations. By taking these steps, policymakers can help to mitigate the impacts of land cover degradation and protect the environment ultimately contributing a land degradation neutral world.

Conclusions

This study aimed to show how land degradation forecasts can be made in the Trends.Earth module using the CA–Markov model. This addresses the issue of the lack of forecasts in the Trends.Earth module, which is a global platform used for reporting to the Global Environment Facility (GEF) and United Nations Convention to Combat Desertification (UNCCD). The study also highlighted the differences between locally produced maps and the global ESA CCI LCLU maps in LCLU assessments. The study assessed the historical and forecasted LCD in UZB from 1993 to 2043, surpassing the target year of 2030 for reporting to the Global Environment Facility (GEF) and the United Nations Convention to Combat Desertification (UNCCD). The additional information (for the period 2033–2043) can be utilised for planning purposes and implementing specific interventions aimed at reversing the degradation in UZB. The following conclusions have been deduced from the study:

A comparison of user accuracy, producer accuracy, and kappa coefficients showed that the locally produced LCLU maps were more accurate than the global ESA CCI LCLU product. This is because the locally classified LCLU maps benefited from the use of local knowledge and an increased number of field points for training data and validation. Therefore, our study shows that for a more accurate and enhanced representation of land degradation results at the local or regional level, it is preferable to use locally produced LCLU maps using high-resolution imagery such as Landsat data, with a sufficient number of representative training data.

Although there are no global-level forecasted ESA CCI LCLU maps available for assessing future land cover

degradation in the Trends.Earth module, this limitation can be overcome by using models, such as the CA–Markov model, which have the capacity to accurately forecast LCLU. Understanding the potential future changes in LCLU and the resulting land degradation is key to informing targeted interventions to reverse land degradation at a local or regional level and contribute to achieving a degradation-neutral world as envisioned by the United Nations.

Between 2023 and 2043, the UZB is predicted to experience a net reduction of approximately 3.2 million hectares of forest cover, with an average annual reduction rate of − 0.13%. In terms of land cover degradation, the UZB is forecasted to remain generally stable, with 87% and 96% of the total land cover area expected to be stable during the periods 2023–2033 and 2033–2043, respectively, relative to the base years 2023 and 2033.

The forest cover in the UZB catchment has been declining and is projected to continue decreasing due to the conversion of forests to grassland, cropland, and built-up land. The degradation of land cover in UZB will persist and necessitates targeted policy interventions to slow down this activity and preserve the ecological and hydrological integrity of the catchment area.

The results of this study are a demonstration of the innovation of making forecasts of LCD in the Trends. Earth module. Therefore, forecasted LCLU products from more accurate forecasting models other than the CA-Markov can be used as inputs in the Trends.Earth module to achieve the desired LCD outcomes.

Supplementary Information

The online version contains supplementary material available at https://doi.org/10.1186/s40068-024-00355-6.

Additional file 1.

Acknowledgements
Not applicable

Author contributions
HMZ: Conceptualisation, data collection, data processing, formal analysis, methodology, software, writing original draft, validation, visualisation. KB and IN: Review & editing, Supervision, Resources, Funding SM: Editing, Validation, Review. All authors read and approved the final manuscript.

Funding
This work was carried out with partly the support of the African Union and European Union under the Wetland Monitoring and Assessment (WeMAST) project and the Transformative Environmental Monitoring to Boost Observations (TEMBO) in Africa project also with funding from the European Union under Grant agreement ID: 101086209. The funding body(s) did not play any role in the design of the study and collection, analysis, and interpretation of data and in writing the manuscript.

Availability of data and materials
The datasets used and/or analysed during the current study are available from the corresponding author on reasonable request. Landsat satellite imagery is available online on https://app.climateengine.org/climateEngine. Landsat satellite imagery are available online on USGS explorer at https://earthexplorer.usgs.gov/. ESA CCI LCLU product is available on the Trends.Earth plugin in QGIS 3.32.3. Trends. Earth module is available as an open-source plugin in QGIS.

Declarations

Ethics approval and consent to participate
Not applicable.

Consent for publication
Not applicable.

Competing interests
The authors declare that they have no competing interests.

Received: 3 May 2024 Accepted: 18 June 2024
Published online: 14 July 2024

References

Abdulrahman AI, Ameen SA (2020) Predicting Land use and land cover spatiotemporal changes utilizing CA-Markov model in Duhok district between 1999 and 2033. Acad J Nawroz Univ 9(4):71. https://doi.org/10.25007/ajnu.v9n4a892

Ahmad A, Quegan S (2012) Analysis of maximum likelihood classification on multispectral data. Appl Mathematical Sci 6:6425

Akdeniz HB,Sag NS (2022) Analysis of land use/land cover changes and prediction of future changes with land change modeler: case of Belek, Turkey. https://doi.org/10.21203/rs.3.rs-1823691/v1

Anderson JR, Ernest E Hardy, John T Roach, and Richard E Witmer. 1976. 'A land use and land cover classification system for use with remote sensor data'. 964. Circular 671. Virginia, USA

Arfasa GF, Owusu-Sekyere E, Doke DA (2023) 'Predictions of land use/land cover change, drivers, and their implications on water availability for irrigation in the Vea catchment Ghana.' Geocarto Int. https://doi.org/10.1080/10106049.2023.2243093

Asif M, Kazmi JH, Tariq A, Zhao N, Guluzade R, Soufan W, Almutairi KF, El Sabagh A, Aslam M (2023) Modelling of land use and land cover changes and prediction using CA-markov and random forest. Geocarto Int. https://doi.org/10.1080/10106049.2023.2210532

Assede ESP, Orou H, Biaou SSH, Geldenhuys CJ, Ahononga FC, Chirwa PW (2023) Understanding drivers of land use and land cover change in Africa: a review. Curr Landscape Ecol Reports 8(2):62–72. https://doi.org/10.1007/s40823-023-00087-w

Baidoo R, Arko-Adjei A, Poku-Boansi M (2023) Land use and land cover changes implications on biodiversity in the Owabi catchment of Atwima Nwabiagya North District, Ghana. Heliyon. https://doi.org/10.1016/j.heliyon.2023.e15238

Bajocco S, De Angelis A, Perini L, Ferrara A, Salvati L (2012) The Impact of land use/land cover changes on land degradation dynamics: a mediterranean case study. Environ Manage 49(5):980–989. https://doi.org/10.1007/s00267-012-9831-8

Banda MA, Banda K, Sakala E, Chomba M, Basin S (2023) Assessment of land use change in the wetland of Barotse floodplain, Zambezi River Sub-Basin, Zambia. Nat Hazards 115:1193–1211. https://doi.org/10.1007/s11069-022-05589-0

Bär V, Akinyemi FO, Speranza CI (2023) Land cover degradation in the reference and monitoring periods of the SDG land degradation neutrality indicator for Switzerland. Ecol Indicat. https://doi.org/10.1016/j.ecolind.2023.110252

Barati AA, Zhoolideh M, Hossein Azadi J, Lee H, Scheffran J (2023) Interactions of land-use cover and climate change at global level: how to mitigate the environmental risks and warming effects. Ecol Indicat. https://doi.org/10.1016/j.ecolind.2022.109829

Bayas JC, Laso LS, Perger C, Justice C, Nakalembe C, Dempewolf J, Fritz S (2017) Validation of automatically generated global and regional cropland data

sets: the case of Tanzania. Remote Sens. https://doi.org/10.3390/rs9080815

Berto F, Jacopo T (2023) Stanford Encyclopedia of Philosophy. In: Edward N. Zalta and Uri Nodelman (eds) Stanford Encyclopedia of Philosophy. Winter 2023. https://plato.stanford.edu/archives/win2023/entries/cellular-automata/

Bogoliubova A, Tymków P (2014) Accuracy assessment of automatic image processing for land cover classification of St. petersburg protected area* 1. Acta Sci Pol 13(1):5–22

Chander G, Markham B (2003) Revised landsat-5 TM radiometrie calibration procedures and postcalibration dynamic ranges. IEEE Trans Geosci Remote Sens 41(11 PART II):2674–2677. https://doi.org/10.1109/TGRS.2003.818464

Chomba I, Banda K, Winsemius CH, Makungu E, Sichingabula HM, Nyambe IA (2022) Coupling hydrologic-hydrodynamic processes in a groundwater dependent tropical floodplain: case of barotse floodplain integrated hydrologic-hydrodynamic inundation modeling in a groundwater dependent tropical floodplain. J Human Earth Future. https://doi.org/10.22541/au.165212270.01201352/v1

Chundu ML, Banda K, Lyoba C, Tembo G, Sichingabula HM, Nyambe IA (2024) Modeling land use/land cover changes using quad hybrid machine learning model in Bangweulu wetland and surrounding areas, Zambia. Environ Chall 14(January):100866. https://doi.org/10.1016/j.envc.2024.100866

Corner RJ, Dewan AM, Chakma S (2014) Monitoring and prediction of land-use and land-cover (LULC) change. In: Dewan A, Corner R (eds) Dhaka megacity geospatial perspectives on urbanisation environment and health. Springer, Netherlands, Heidelberg, pp 75–97. https://doi.org/10.1007/978-94-007-6735-5_5

Cowie AL, Orr BJ, Castillo VM, Sanchez PC, Crossman ND, Erlewein A, Louwagie G et al (2018) Land in balance: the scientific conceptual framework for land degradation neutrality. Environ Sci Policy 79(January):25–35. https://doi.org/10.1016/j.envsci.2017.10.011

Duarte D, Fonte C, Costa H, Caetano M (2023) Thematic comparison between ESA World Cover 2020 land cover product and a national land use land cover map. Land. https://doi.org/10.3390/land12020490

DB Fanshawe, JR Timberlake, MG Bingham (2010) 'Vegetation descriptions of the upper Zambezi districts of Zambia vegetation descriptions of the upper Zambezi districts of Zambia originally issued as forest research pamphlets by the Zambia forest research department, Kitwe, Zambia'.

Ferreira CSS, Seifollahi-Aghmiuni S, Destouni G, Ghajarnia N, Kalantari Z (2022) 'Soil degradation in the European Mediterranean region processes Status and Consequences.' Sci Total Environ. https://doi.org/10.1016/j.scitotenv.2021.150106

Foody GM (2002) Status of Land cover classification accuracy assessment. Remote Sens Environ 80:185–201

Friedl MA, Woodcock CE, Olofsson PS, Zhu Z, Loveland T, Stanimirova R, Arevalo P et al (2022) Medium spatial resolution mapping of global land cover and land cover change across multiple decades from landsat. Front Remote Sens. https://doi.org/10.3389/frsen.2022.894571

García-Álvarez D, Olmedo MTC, Paegelow M, Mas JF (2022) Validation practices with QGIS land use cover datasets and validation tools. In: García-Álvarez D, Olmedo MTC, Paegelow M, Mas JF (eds) Land use cover datasets and validation tools validation practices with QGIS. Springer, Cham

Gashaw T, Tulu T, Argaw M, Worqlul AW (2017) 'Evaluation and prediction of land use/land cover changes in the Andassa watershed, Blue Nile Basin, Ethiopia.' Environ Syst Res. https://doi.org/10.1186/s40068-017-0094-5

Gebresamuel G, Bal RS, Øystein D (2010) Land-use changes and their impacts on soil degradation and surface runoff of two catchments of Northern Ethiopia. Acta Agric Scand Sect B Soil Plant Sci 60(3):211–226. https://doi.org/10.1080/09064710902821741

Gharaibeh A, Shaamala A, Obeidat R, Al-Kofahi S (2020) Improving land-use change Modeling by integrating ANN with cellular automata-Markov chain model. Heliyon. https://doi.org/10.1016/j.heliyon.2020.e05092

Ghosh P, Mukhopadhyay A, Chanda A, Mondal P, Akhand A, Mukherjee S, Nayak SK et al (2017) Application of cellular automata and markov-chain model in geospatial environmental modelling—a review. Remote Sens Appl Soc Environ. https://doi.org/10.1016/j.rsase.2017.01.005

Halmy MW, Gessler PE, Hicke JA, Salem BB (2015) Land use/land cover change detection and prediction in the north-western coastal desert of Egypt using Markov-CA. Appl Geogr 63(September):101–112. https://doi.org/10.1016/j.apgeog.2015.06.015

Hamad R, Balzter H, Kolo K (2018) Predicting land use/land cover changes using a CA-Markov model under two different scenarios. Sustainability (switzerland). https://doi.org/10.3390/su10103421

Herrmann SM, Brandt M, Rasmussen K, Fensholt R (2020) Accelerating land cover change in West Africa over four decades as population pressure increased. Commun Earth Environ. https://doi.org/10.1038/s43247-020-00053-y

Hu X, Næss JS, Iordan CM, Huang B, Zhao W, Cherubini F (2021) Recent global land cover dynamics and implications for soil erosion and carbon losses from deforestation. Anthropocene 34. https://doi.org/10.1016/j.ancene.2021.100291

Hughes DA, Farinosi F (2020) 'Assessing development and climate variability impacts on water resources in the Zambezi river basin simulating future scenarios of climate and development.' J Hydrol Reg Stud. https://doi.org/10.1016/j.ejrh.2020.100763

Islami FA, Tarigan SD, Wahjunie ED, Dasanto BD (2022) Accuracy assessment of land use change analysis using google earth in Sadar watershed Mojokerto regency. IOP Conf Series Earth Environ Sci. https://doi.org/10.1088/1755-1315/950/1/012091

Kamusoko C, Aniya M, Adi B, Manjoro M (2009) Rural Sustainability under threat in Zimbabwe—simulation of future land use/cover changes in the Bindura district based on the Markov-cellular automata model. Appl Geogr 29(3):435–447. https://doi.org/10.1016/j.apgeog.2008.10.002

Karan SK, Samadder SR (2018) A comparison of different land-use classification techniques for accurate monitoring of degraded coal-mining areas. Environ Earth Sci. https://doi.org/10.1007/s12665-018-7893-5

Kayitesi NM, Guzha AC, Mariethoz G (2022) Impacts of land use land cover change and climate change on river hydro-morphology—a review of research studies in tropical regions. J Hydrol. https://doi.org/10.1016/j.jhydrol.2022.128702

Kgaphola MJ, Ramoelo A, Odindi J, Mwenge Kahinda JM, Seetal AR, Musvoto C (2023) Impact of land use and land cover change on land degradation in rural semi-arid south Africa: case of the greater Sekhukhune district municipality. Environ Monit Assess. https://doi.org/10.1007/s10661-023-11104-0

Kim I, Le QB, Park SJ, Tenhunen J, Koellner T (2014) Driving forces in archetypical land-use changes in a mountainous watershed in East Asia. Land 3(3):957–980. https://doi.org/10.3390/land3030957

Kindu M, Schneider T, Teketay D, Knoke T (2015) Drivers of land use/land cover changes in munessa-shashemene landscape of the South-Central highlands of Ethiopia. Environ Monit Assess. https://doi.org/10.1007/s10661-015-4671-7

Kissanga R, Catarino L, Máguas C, Cabral AIR (2024) Dynamics of land-cover change and characterization of charcoal production and trade in southwestern Angola. Remote Sens Appl Soc Environ. https://doi.org/10.1016/j.rsase.2024.101162

Kleemann J, Baysal G, Bulley HNN, Fürst C (2017) Assessing driving forces of land use and land cover change by a mixed-method approach in North-Eastern Ghana, West Africa. J Environ Manage 196(July):411–442. https://doi.org/10.1016/j.jenvman.2017.01.053

Kouassi JL, Gyau A, Diby L, Bene Y, Kouamé C (2021) 'Assessing land use and land cover change and farmers' perceptions of deforestation and land degradation in South-West Côte d'Ivoire, West Africa'. Land. https://doi.org/10.3390/land10040429

Lam NS-N, Liang S (2008) Methodologies for mapping land cover/land use and its change. Springer, Netherlands, Dordrecht, pp 341–367

Latham JS, He C, Alinovi L, DiGregorio A, Kalensky Z (2002) FAO Methodologies for Land Cover Classification and Mapping. In: Walsh SJ, Crews-Meyer KA (eds) Linking People, Place, and Policy. Springer, Boston, MA. https://doi.org/10.1007/978-1-4615-0985-1_13

Lesiv M, See L, Mora B, Pietsch S, Fritz S, Bun H, Sendabo D (2019) Accuracy assessment of the ESA CCI land cover map: Kenya, Gabon, Ivory Coast and South Africa. www.iiasa.ac.at.

Lewandowski Z, Dent D, Wu Y, De Jong R (2013) Land Degradation and Ecosystem Services. In: Lal R, Lorenz K, Hüttl RF, Schneider BU, von Braun J (eds) Ecosystem services and carbon sequestration in the biosphere. Springer, Netherlands, Dordrecht, pp 357–381

Lillesand MT, Kiefer WR, Chipman WJ (2015) Remote Sensing and Image Interpretation. 7th Edition. In: Photogrammetric Engineering & Remote Sensing 81(8). https://doi.org/10.14358/PERS.81.8.615
Liping C, Yujun S, Saeed S (2018) 'Monitoring and predicting land use and land cover changes using remote sensing and GIS Techniques—a case study of a Hilly Area, Jiangle, China.' PLoS ONE. https://doi.org/10.1371/journal.pone.0200493
Lukas P, Melesse AM, Kenea TT (2023) 'Prediction of Future land use/land cover changes using a coupled CA-ANN model in the upper Omo-Gibe River basin, Ethiopia.' Remote Sens. https://doi.org/10.3390/rs15041148
Lulla K, Duane Nellis M, Rundquist B, Srivastava PK, Szabo S (2021) Mission to Earth LANDSAT 9 will continue to view the world. Geocarto Int. https://doi.org/10.1080/10106049.2021.1991634
Maitima JM, Mugatha SM, Reid RS, Gachimbi LN, Majule A, Lyaruu H, Pomery D, Mathai S, Mugisha S (2009) The linkages between land use change, land degradation and biodiversity across East Africa. Afr J Environ Sci Technol 3(10):310–325. https://doi.org/10.5897/AJEST08.173
Makungu E, Hughes DA (2021) Understanding and Modelling the effects of wetland on the hydrology and water resources of large African River Basins. J Hydrol. https://doi.org/10.1016/j.jhydrol.2021.127039
Memarian H, Balasundram SK, Talib JB, Sung CTB, Sood AM, Abbaspour K (2012) Validation of CA-Markov for simulation of land use and cover change in the Langat basin, Malaysia. J Geogr Inf Syst 04(06):542–554. https://doi.org/10.4236/jgis.2012.46059
Mendelsohn JM (2019) Landscape changes in angola. In: Huntley BJ, Russo V, Lages F, Ferrand N (eds) Biodiversity of Angola: science and conservation: a modern synthesis. Springer International Publishing, Cham, pp 123–137
Mishra VN, Rai PK, Prasad R, Punia M, Nistor MM (2018) Prediction of Spatio-temporal land use/land cover dynamics in rapidly developing Varanasi district of Uttar Pradesh, India, using geospatial approach: a comparison of hybrid models. Appl Geomat 10(3):257–276. https://doi.org/10.1007/s12518-018-0223-5
Mondal S, Sharma N, Garg PK, Kappas M (2016) Statistical independence test and validation of CA Markov land use land cover (LULC) prediction results. Egypt J Remote Sens Space Sci 19(2):259–272. https://doi.org/10.1016/j.ejrs.2016.08.001
Mondal MS, Sharma N, Kappas M, Garg PK (2019) Ca Markov modeling of land use land cover dynamics and sensitivity analysis to identify sensitive parameter(s). Int Archiv Photogramm Remote Sens Spatial Inform Sci 42:723–729
Mwampamba TH, Abrams RW, Awoyemi S, Babalola FD, Borokini TI, Egoh B, Idrissi HR, Koussa T, Nganje M, O'Leary J (2016) The implications of globalization for conservation in Africa. Afr J Ecol. https://doi.org/10.1111/aje.12322
Näschen K, Diekkrüger B, Evers M, Höllermann B, Steinbach S, Thonfeld F (2019) The impact of land use/land cover change (LULCC) on water resources in a tropical catchment in Tanzania under different climate change scenarios. Sustainability. https://doi.org/10.3390/su11247083
Norovsuren B, Tseveen B, Batomunkuev V, Renchin T, Natsagdorj E, Yangiv A, Mart Z (2019) Land cover classification using maximum likelihood method (2000 and 2019) at Khandgait valley in Mongolia. IOP Conf Series Earth Environ Sci. https://doi.org/10.1088/1755-1315/381/1/012054
Nyatuame M, Agodzo S, Amekudzi LK, Mensah-Brako B (2023) Assessment of past and future land use/cover change over Tordzie Watershed in Ghana. Front Environ Sci. https://doi.org/10.3389/fenvs.2023.1139264
Olofsson P, Foody GM, Herold M, Stehman SV, Woodcock CE, Wulder MA (2014) Good practices for estimating area and assessing accuracy of land change. Remote Sens Environ. https://doi.org/10.1016/j.rse.2014.02.015
Orr BJ, Cowie AL, Castillo Sanchez VM, Chasek P, Crossman ND, Erlewein A, Louwagie G, Maron M, Metternicht GI, Minelli S, Tengberg AE, Walter S, Welton S (2017) Scientific Conceptual Framework for Land Degradation Neutrality. A Report of the Science-Policy Interface. United Nations Convention to Combat Desertification (UNCCD), Bonn, Germany. https://www.unccd.int/resources/publications/achieving-land-degradation-neutrality-country-level-building-blocks-ldn
Padma S, Sanjeevi S (2014) Jeffries Matusita based mixed-measure for improved Spectralmatching in hyperspectral image analysis. Int J Appl Earth Obs Geoinf 32(1):138–151. https://doi.org/10.1016/j.jag.2014.04.001
Perumal K, Bhaskaran R (2010) Supervised classification performance of multi-spectral images. J Comput 2(2):124–129
Phiri D, Morgenroth J, Cong X (2019) Long-Term land cover change in zambia: an assessment of driving factors. Sci Total Environ. https://doi.org/10.1016/j.scitotenv.2019.134206
Potapov P, Hansen MC, Pickens A, Hernandez-Serna A, Tyukavina A, Turubanova S, Zalles V et al (2022) The global 2000–2020 land cover and land use change dataset derived from the Landsat archive: first results. Front Remote Sens. https://doi.org/10.3389/frsen.2022.856903
Reinhart V, Fonte CC, Hoffmann P, Bechtel B, Rechid D, Boehner J (2021) Comparison of ESA climate change initiative land cover to CORINE land cover over eastern Europe and the Baltic states from a regional climate modeling perspective. Int J Appl Earth Observat Geoinform. https://doi.org/10.1016/j.jag.2020.102221
Richard B (2012) 'A risky climate for southern African hydro. Int Rivers. https://doi.org/10.13140/RG.2.2.30193.48486
Roy DP, Wulder MA, Loveland TR, Woodcock CE, Allen RG, Anderson MC, Helder D et al (2014) Landsat-8: science and product vision for terrestrial global change research. Remote Sens Environ 145(April):154–172. https://doi.org/10.1016/j.rse.2014.02.001
Roy S, Farzana K, Papia M, Hasan M (2015) Kappa statistics 1989 (88.67), 2000 (92.33) and 2014 (89.67) respectively. Int J Sci Basic Appl Res 24(4):125–148
Rwanga SS, Ndambuki JM (2017) Accuracy Assessment of land use/land cover classification using remote sensing and GIS. Int J Geosci 08(04):611–622. https://doi.org/10.4236/ijg.2017.84033
Sang L, Zhang C, Yang J, Zhu D, Yun W (2011) Simulation of land use spatial pattern of towns and villages based on CA-Markov model. Math Comput Model 54(3–4):938–943. https://doi.org/10.1016/j.mcm.2010.11.019
Sen R, Goswami S, Chakraborty B (2019) Jeffries-Matusita distance as a tool for feature selection. In: International Conference on Data Science and Engineering (ICDSE), Patna, India, 2019, pp. 15–20. https://doi.org/10.1109/ICDSE47409.2019.8971800
Shakachite O, Chungu D, Ng'andwe AM, Siampale P, Chendauka B, Vesa WJ, Roberts L (2016) Integrated land use assessment phase II—report for Zambia. The food and agriculture organization of the united nations and the forestry department, Ministry of Lands and Natural Resources, Lusaka, Zambia. 1–122.
Shivakumar BR, Rajashekararadhya SV (2018) Investigation on land cover mapping capability of maximum likelihood classifier: a case study on North Canara, India. Proced Comput Sci 143:579–586. https://doi.org/10.1016/j.procs.2018.10.434
Singh SK, Mustak Sk, Srivastava PK, Szabó S, Islam T (2015) Predicting spatial and decadal LULC changes through cellular automata Markov chain models using earth observation datasets and geo-information. Environ Process 2(1):61–78. https://doi.org/10.1007/s40710-015-0062-x
Strahler AH, Boschetti L, Foody GM, Friedl MA, Hansen MC, Herold M, Mayaux P, Morisette JT, Stehman SV, Woodcock CE (2006) Global Land Cover Validation: Recommendations for Evaluation and Accuracy Assessment of Global Land Cover Maps. European Commission, Directorate-General Joint Research Centre, Institute of Environment and Sustainability. https://www.researchgate.net/publication/238580124
Swain PH, King RC (1973) Two effective feature selection criteria for multispectral remote sensing. In: The International Joint Conference on Pattern Recognition, pp 1–7. http://docs.lib.purdue.edu/larstech. http://docs.lib.purdue.edu/larstech/39
Tiamgne XT, Kalaba FK, Nyirenda VR (2021) Land use and cover change dynamics in Zambia's Solwezi copper mining district. Sci Afr. https://doi.org/10.1016/j.sciaf.2021.e01007
Timberlake J (2000) Biodiversity of the Zambezi Basin. Biodivers Found Africa 9:1–20
Trends.Earth (2022) Conservation International. Available online at: http://trends.earth
Tulbure MG, Hostert P, Kuemmerle T, Broich M (2022) Regional matters: on the usefulness of regional land-cover datasets in times of global change. Remote Sens Ecol Conserv 8(3):272–283. https://doi.org/10.1002/rse2.248
Ukhurebor KE, Aigbe UO, Onyancha RB, Ndunagu JN, Osibote OA, Emegha JO, Balogun VA, Kusuma HS, Darmokoesoemo H (2022) An overview of the emergence and challenges of land reclamation issues and prospect. Appl Environ Soil Sci. https://doi.org/10.1155/2022/5889823
Vesa L, Bassil M, Chendauka B, Siampale A, Wamunyima S, Mukosha J, Chileshe F, Sokatela S, Mbindo K, Tavani R, Fox J (2013) Integrated Land Use Assessment Phase II Zambia. In: Biophysical Field Manual. Forestry

Department, Ministry of Lands, Natural Resources and Environmental Protection, pp 40–46
Wang L, Bartlett P, Pouliot D, Chan E, Lamarche C, Wulder MA, Defourny P, Brady M (2019) Comparison and assessment of regional and global land cover datasets for use in CLASS over Canada. Remote Sens. https://doi.org/10.3390/rs11192286
Wang SW, Gebru BM, Lamchin M, Kayastha RB, Lee WK (2020) Land use and land cover change detection and prediction in the Kathmandu district of Nepal using remote sensing and GIS. Sustainability (switzerland). https://doi.org/10.3390/su12093925
Wang SW, Munkhnasan L, Lee WK (2021) 'Land use and land cover change detection and prediction in Bhutan's high altitude City of Thimphu, using cellular automata and Markov Chain.' Environ Chall. https://doi.org/10.1016/j.envc.2020.100017
Winkler K, Fuchs R, Rounsevell M, Herold M (2021) Global land use changes are four times greater than previously estimated. Nat Commun. https://doi.org/10.1038/s41467-021-22702-2
World Bank (2010) The Zambezi river basin a multi-sector investment opportunities analysis state of the basin. World Bank, Washington DC
Zimba H, Kawawa B, Chabala A, Phiri W, Selsam P, Meinhardt M, Nyambe I (2018) Assessment of trends in inundation extent in the Barotse floodplain, upper Zambezi river basin: a remote sensing-based approach. J Hydrol Reg Stud 15(February):149–170. https://doi.org/10.1016/j.ejrh.2018.01.002

Publisher's Note